energies

MDPI

Article

Performance Investigation of Currently Available Reaction Mechanisms in the Estimation of NO Measurements: A Comparative Study

Ali Alnasif [1,2,*], Syed Mashruk [1], Masao Hayashi [3,4], Joanna Jójka [5], Hao Shi [1], Akihiro Hayakawa [3] and Agustin Valera-Medina [1,*]

1 College of Physical Sciences and Engineering, Cardiff University, Queen's Building, Cardiff CF24 3AA, UK
2 Engineering Technical College of Al-Najaf, Al-Furat Al-Awsat Technical University, Najaf 31001, Iraq
3 Institute of Fluid Science, Tohoku University, 2-1-1 Katahira, Aoba-ku, Sendai 980-8577, Japan
4 Department of Aerospace Engineering, Tohoku University, 6-6-1, Aoba, Aramaki, Aoba-ku, Sendai 980-8579, Japan
5 Institute of Thermal Engineering, Poznan University of Technology, 60-965 Poznan, Poland
* Correspondence: alnasifah@cardiff.ac.uk (A.A.); valeramedinaa1@cardiff.ac.uk (A.V.-M.)

Abstract: Ammonia (NH_3) has been receiving the attention of researchers as an alternative promising green fuel to replace fossil sources for energy production. However, the high NOx emissions are one of the drawbacks and restrictions of using NH_3 on a broad scale. The current study investigates NO production/consumption for a 70/30 (vol%) NH_3/H_2 mixture using kinetic reaction mechanism concepts to shed light on the essential reaction routes that promote/inhibit NO formation. Sixty-seven kinetic reaction mechanisms from the literature have been investigated and compared with recently reported measurements at a wide range of equivalence ratios (ϕ) (0.6–1.4), atmospheric pressure and temperature conditions. Both numerical simulations and experimental measurements used the same combustion reactor configuration (premixed stabilized stagnation flame). To highlight the best kinetic model for the predicting of the NO experimental measurements of NO, a symmetric mean absolute percentage error (SMAPE) has been determined as a preliminary estimation by comparing both numerical and experimental measurements. The results found that the kinetic reaction mechanism of Glarborg showed an accurate prediction with a minor error percentage of 2% at all lean and stoichiometric conditions. Meanwhile, the kinetic model of Wang accurately predicted the experimental data with 0% error at ϕ = 1.2 and underestimated the mole fraction of NO at 1.4 ϕ with an error of 10%. The sensitivity analysis and rate of production/consumption of NO mole fractions analysis have also been implemented to highlight the most important reactions that promote/inhibit NO formation. At lean and stoichiometric conditions, Glarborg kinetic model shows that the kinetic reactions of HNO + H ⇌ NO + H_2, HNO + O ⇌ NO + OH, and NH + O ⇌ NO + H are the most important reaction routes with considerable effect on NO formation for 70/30 (vol%) NH_3/H_2 mixture. In contrast, the reactions of NH_2 + NO ⇌ N_2 + H_2O, NH_2 + NO ⇌ NNH + OH, NH + NO ⇌ N_2O + H, and N + NO ⇌ N_2 + O significantly consume NO to N_2, NNH, and N_2O. Further, Wang's mechanism illustrated the dominant effect of each HNO + H ⇌ NO + H_2, N + OH ⇌ NO + H, NH + O ⇌ NO + H in NO formation and NH + NO ⇌ N_2O + H, NH_2 + NO ⇌ NNH + OH, and NH_2 + NO ⇌ N_2 + H_2O in the consumption of NO mole fractions.

Keywords: ammonia; burner-stabilized stagnation flame; kinetic modeling; NO formation/consumption; reaction mechanisms

Citation: Alnasif, A.; Mashruk, S.; Hayashi, M.; Jójka, J.; Shi, H.; Hayakawa, A.; Valera-Medina, A. Performance Investigation of Currently Available Reaction Mechanisms in the Estimation of NO Measurements: A Comparative Study. *Energies* **2023**, *16*, 3847. https://doi.org/10.3390/en16093847

Academic Editor: Ekenechukwu Okafor

Received: 24 March 2023
Revised: 23 April 2023
Accepted: 24 April 2023
Published: 29 April 2023

1. Introduction

Energy plays a crucial role in human life, while the combustion of conventional fuels, such as coal, significantly contributes to most of the total energy production throughout human history. The vast increase in worldwide population and the increase in relevant

industrial processes has contributed to the deterioration of the ecosystem causing environmental issues such as climate change. Carbon dioxide (CO_2) is the most prominent GHG responsible for raising global temperatures, since 30% of the global warming impact is caused due to the production of CO_2 [1]. Due to the role of combustion as an important contributor to GHG emissions, finding fuel sources to attain zero carbon emissions is critical [2]. Both ammonia (NH_3) and hydrogen (H_2) can be used as carbon-free fuels. However, it is preferred to use NH_3 over H_2—in some circumstances—as NH_3 is an efficient H_2 carrier with high gravimetric hydrogen density, which makes it a potential medium for hydrogen storage; further, the handling, transportation, and distribution of NH_3 are comparatively more accessible and safer compared to H_2 [3].

Furthermore, the vast existing infrastructure and the ease of NH_3 liquefication compared to pure H_2 significantly impact transport processes and final costs [4]. Despite the significant advantages provided by NH_3, there are some concerns about the drawbacks represented by the low burning velocity and high nitrogen oxides (NO_x) formation when using this molecule [4]. High-fuel NO_x formation coincides with increasing environmental challenges [3]. The ideal combustion of NH_3 produces only nitrogen (N_2) and water (H_2O) without having NO_x traces [5]. However, in practical combustion systems, NO_x production is substantial, especially under fuel-lean conditions [5].

Similarly, the low burning velocity is a practical challenge. To overcome this drawback of NH_3 and improve its combustion characteristics, it is recommended to blend NH_3 with another fuel such as H_2 [6]. Moreover, as there will be no CO_2 production in the by-products, H_2 can be considered the cleanest additive when mixed with NH_3. In addition, the capability of producing H_2 as a product from the cracking process of NH_3 can have further benefits. The effects of adding H_2 to the NH_3 flames have been investigated experimentally by Choi et al. [7] using counterflow non-premixed NH_3/H_2/air flames. Their study found that the radical pools of H, OH, and O increase when the H_2 fractions increase in the mixture, resulting in an increase in the maximum flame temperatures and the blow-off resistance.

Several experimental studies [8–14] have been carried out on ammonia-based combustion. Tohoku University's studies have focused on developing turbine burners with low-NO_x formation [8,9]. The research group used both pure NH_3 as fuel and blended fuel of NH_3/H_2. Their outcomes showed that the NO mole fraction rapidly decreased in rich conditions, whereas the concentration of unburned NH_3 increased under the same conditions [9]. Additionally, the total NH_3 emission resulting from swirling flows is affected by the unburnt NH_3 flowing nearby the liner wall [9]. Several experimental studies have been performed at Cardiff University, United Kingdom, on H_2/NH_3 blends by using a generic tangential swirl burner to burn a variety of mixtures at different power outputs NH_3 [10–13]. Their studies have investigated various equivalence ratios and blending ratios, such as spectrometric profiles and emissions (NO, N_2O, NO_2, and NH_3). Their finding showed that the maximum concentration of NO hits the peak in lean conditions ($\phi \approx 0.9$) for pure NH_3 and NH_3/H_2 blends.

In contrast, NO_x concentration decreases when moving the equivalence ratio to the leaner or richer conditions, typically more towards the rich side. Studies have shown that the concentration of NH_2 increases at rich conditions, and both NH_2 and NNH have high sensitivity to NO formation/decomposition [13]. Along with this effect, NH_3 oxidation processes and NO_x production were experimentally investigated by Abián et al. [14] using a laboratory quartz tubular flow reactor. The experimental outcomes showed that increasing O_2 levels would decrease the temperature requirements to attain the complete oxidation of NH_3, and high levels of O_2 promote NO formation.

Since NH_3 lacks carbon, NO is the major harmful pollutant from NH_3 combustion. In most cases, the fuel-bound nitrogen is the main contributor to NO_x formation in NH_3 flames rather than the thermal NO_x produced by atmospheric nitrogen [15]. Consequently, a deep understanding of NH_3 combustion chemistry is required. Furthermore, a detailed analysis of NO_x production pathways is necessary to precisely estimate emissions due to

fuel-bound nitrogen. Nowadays, the development and optimization processes on NH_3 as fuel for practical applications such as gas turbines and internal combustion engines are carried out using high-accuracy computer modeling of fluid and gas dynamics of the conversion process inside the combustion chamber. In addition, NH_3, as a promising fuel, needs reliable kinetic mechanisms. The chemical kinetic reaction mechanisms should be based on a comprehensive understanding of the chemical conversion of the fuel and intermediate formations due to fuel oxidation. Several attempts have been made to establish reliable, comprehensive models for NH_3 oxidation [16–18]. The previously established mechanisms [16,18–22] have been used as baseline mechanisms for development and optimization purposes in the oxidation of NH_3 mixtures.

Improving the kinetic mechanisms for NH_3 involves investigating the rate constants parameters of the reactions that have nitrogen-containing species, which in turn contribute considerably to the oxidation process of NH_3. Updating the rate constant parameters and thermochemical data for nitrogen-containing species and highlighting the key gas-phase reactions of NH_3 combustion affect the optimization process of NH_3 oxidation and move it closer to the practical level. Many studies have been carried out in previous years that aimed to improve NH_3 kinetics based on the experimental tests of combustion of NH_3 using several combustion systems, such as burner-stabilized premixed flames, shock-tube, jet-stirred reactors, and plug-flow reactors [23–28]. Nozari and Karabeyoglu [29] developed a kinetic reaction mechanism for predicting the NO_x formation for the combustion of NH_3/H_2 blends, containing detailed nitrogen-related sub-mechanisms, which consisted of 30 species and 240 reactions. Their findings indicate excellent consistency with the experimental measurements and data from the developed model reactions. Another study was carried out by Zhang et al. [30] by implementing a jet-stirred reactor (JSR) to oxidize NH_3/H_2 blends at atmospheric conditions and using the experimental results to develop a kinetic model able to estimate the NO_x measurements reliably. Based on the analysis of their developed model, they found that H_2 effectively impacts the nitrogen-related radicals (NH_2, NH, and N), where the concentration of these radicals decreases when the H_2 blending ratio increases, which, in turn, reduces NO formation. Conversely, the promotion of the oxygenated radicals (O, OH, and HO_2) has improved with an increasing H_2 level resulting in the enhancement of NO formation.

Recently, a comprehensive study was carried out by András et al. [31] by investigating the performance of 18 recently published kinetic reaction mechanisms using a wide range of experimental measurements reported by previous studies of different fuel combinations of pure NH_3, NH_3/H_2, and NH_3/syngas blends. The experimental measurements included a data set of ignition delay times measured in a shock tube, concentration measurements in jet-stirred (JSR) and flow reactors (FR), and laminar burning velocity measurements. Their methodology has included a quantitative method that compared the outcomes of the tested mechanisms to the collected experimental measurements using a unique framework code, Optima ++. A sensitivity analysis of the best-performing kinetic models determined the most influential model parameters based on the simulation outcomes. Their findings showed that although essential reactions are not the same for different types of combustion experiments, most of these reactions contain NH_3, NH_2, and NNH species. Furthermore, the radical species of H, O, OH, HO_2, NH_3, NH_2, O_2, and H_2 have the most sensitive effect on thermodynamic properties.

Although numerous attempts have been made to improve the accuracy of model predictions, the optimization for the developed models has been restricted to specific conditions. Additionally, the enhancement process must be comprehensive and rely on massive data sets of experimental measurements with broad boundary conditions for the combustion of NH_3 and its blends. Therefore, the current study aims to investigate combustion chemistry's performance in kinetic modeling of a 70/30 (vol%) NH_3/H_2 mixture. The investigation process includes the following steps: (1) utilization of recently reported NO measurements by Hayakawa et al. [32], which is based on using stagnation flame configurations for accurate measurements employing better-collected samples, especially

at very lean conditions where maximum NO formation takes place, as well as to avoid stabilization issues which take place at lean conditions of NH_3-based fuels [9,32–34]; (2) modeling of 67 kinetic reaction mechanisms from the literature by studying their performance in the estimation of NO mole fractions at atmospheric conditions of pressure and temperature and various equivalence ratio (0.6–1.4); and (3) applying symmetric mean absolute percentage error (SMAPE) analyses for a preliminary estimation to highlight the best-performing kinetic model for the estimation of NO mole fractions at lean, stoichiometric, and rich conditions.

2. Numerical Setup and Kinetic Modeling

Sixty-seven chemical kinetic mechanisms have been analyzed numerically by ANSYS Chemkin-PRO 2022 R2 software. A burner-stabilized stagnation flame model was adopted in this study. All numerical simulations have been implemented in a one-dimensional computational model 2 cm in length that mimics the same distance applied from experiments (the distance from the nozzle burner to the top plate). For all tested cases, the grid properties, such as the maximum number of grid points allowed and the adaptive grid control based on solution gradient and curvature, were set to 5000, 0.01, and 0.01. This study has also considered mesh dependency to achieve precise results. Table 1 shows each tested mechanism in terms of the number of species and reactions.

To avoid stabilization issues and obtain accurate measurements, a stagnation flame configuration has been used to determine the mole fraction of NO from the combustion of 70/30 (vol%) NH_3/H_2 blended fuel. Experimental work has been carried out at Tohoku University using a stagnation flame configuration. The detail of the experimental setup can be found elsewhere [32]. Ammonia and hydrogen were used as fuel, and the air was used as an oxidizer. All the experimental tests have been conducted under atmospheric conditions (T = 295 K, P = 1 atm). The experimental measurements of NO concentration have been employed for various equivalence ratios, ϕ. A top stagnation plate was mounted 2 cm above the burner outlet to generate a stagnation flow. The values of the top plate surface temperature (T_w) and the mixture inlet velocity (V_{in}) were varied due to the variation in equivalence ratios, which caused the laminar burning velocity to change. Experimental measurements from [32] were selected regarding the same condition of interest, such as the mole fraction of hydrogen in the fuel, the range of the equivalence ratio, and the standard conditions of the unburned gas.

A symmetric mean absolute percentage error (SMAPE) formula was utilized [35] to determine the optimal kinetic reaction mechanism with superior performance compared to experimental measurements [32]. This formula involved computing the discrepancy between the experimental measurements and the numerical simulation, thereby generating more accurate estimations of the selected mechanism's performance across various equivalence ratios, as specified in Equation (1).

It is worth noting that the SMAPE method is preferred for error estimation when the actual value reported by experiments is close to zero [36]. This preference arises from the sensitivity of error estimates to small values reported by experiments, which may lead to a reduction in estimation accuracy. This phenomenon can be observed in the absolute percentage error (APE) when utilized as a means of error estimation.

$$\text{SMAPE} = \frac{|F_t - A_t|}{(A_t + F_t)} * 100\% \quad (1)$$

where F_t is the forecasting value standing for numerical calculations, and A_t is the actual value from experiments.

Table 1. Kinetic reaction mechanisms adopted in the present study.

No.	Kinetic Mechanism	No. of Reactions	No. of Species	Ref.	No.	Kinetic Mechanism	No. of Reactions	No. of Species	Ref.
1	Bertolino et al., 2021	264	38	[37]	35	Dagaut et al., 2008	250	41	[38]
2	Mei et al., 2021	264	38	[39]	36	Gregory P. Smith et al., 2000	325	53	[40]
3	Han et al., 2021	298	36	[41]	37	Coda Zabetta and Hupa, 2008	371	60	[42]
4	Mei, et al., 2021	257	40	[27]	38	Alzueta MU, 2016	654	131	[43]
5	Gotama et al., 2022	119	26	[24]	39	Shmakov et al., 2010	1207	127	[44]
6	Shrestha et al., 2021	1099	125	[25]	40	Esarte et al., 2011	536	79	[45]
7	Z. Wang et al., 2021	444	91	[46]	41	Abian et al., 2015	201	31	[47]
8	X. Zhang et al., 2021	263	38	[30]	42	T. Wang et al., 2018	925	81	[48]
9	Arunthanayothin et al., 2021	2444	157	[49]	43	T. Faravelli, 2017	158	29	[50]
10	Stagni et al., 2020	203	31	[23]	44	POLIMI, 2014	155	29	[51]
11	Han et al., 2019	177	35	[52]	45	Marques et al., 2009	318	61	[53]
12	De Persis et al., 2020	647	103	[54]	46	Aranda et al., 2013	566	95	[55]
13	Mei et al., 2019	265	38	[56]	47	Jiang et al., 2020	60	19	[57]
14	Li et al., 2019	957	128	[28]	48	Sun et al., 2022	486	66	[58]
15	Okafor et al., 2019	356	59	[59]	49	Song et al., 2019	158	29	[60]
16	Glarborg et al., 2018	231	39	[61]	50	Mével et al., 2009	203	32	[62]
17	Shrestha et al., 2018	1081	124	[63]	51	Da Rocha et al., 2019 (Improved Mathiue mech.)	66	22	[64]
18	Otomo et al., 2018	213	32	[65]	52	Da Rocha et al., 2019 (Improved Otomo mech.)	51	21	[64]
19	U. Mechanism, 2018	41	20	[66]	53	Da Rocha et al., 2019 (Improved Okafor mech.)	70	24	[64]
20	Klippenstein et al., 2018	211	33	[67]	54	Kovaleva et al., 2022	354	59	[68]
21	Nakamura et al., 2017	232	33	[69]	55	Houshfar et al., 2012 (Midd temp.)	91	26	[70]
22	Y. Zhang et al., 2017	251	44	[71]	56	Houshfar et al., 2012 (High temp.)	430	52	[70]
23	Lamoureux et al., 2016	934	123	[72]	57	Houshfar et al., 2012 (Low temp.)	198	35	[70]
24	Xiao et al., 2017	276	55	[73]	58	Capriolo et al., 2021	2300	201	[74]
25	Song et al., 2016	204	32	[75]	59	Xu et al., 2023	389	69	[76]
26	Nozari and Karabeyoğlu, 2015	91	21	[29]	60	Thomas et al., 2022	1099	125	[77]
27	Mathieu and Petersen, 2015	278	54	[78]	61	Kovács et al., 2020	214	34	[79]
28	Duynslaegher et al., 2012	80	19	[80]	62	Kovács et al., 2021	537	70	[81]
29	Klippenstein et al., 2011	202	31	[82]	63	K. Zhang et al., 2011	701	88	[83]
30	Saxena and Williams, 2007	288	59	[84]	64	Lamoureux et al., 2010	883	119	[85]
31	Valkó et al., 2022	537	70	[86]	65	Konnov, 2009	1207	127	[16]
32	Alzueta et al., 2001	464	65	[87]	66	Mendiara and Glarborg, 2009	779	79	[88]
33	Nakamura and Shindo, 2019	485	66	[89]	67	Tian et al., 2009	703	84	[26]
34	Glarborg, 2022	270	41	[90]					

3. Results and Discussion

Figure 1 refers to the data estimated numerically by Chemkin-Pro 2022 R2 software for 67 chemical kinetic reaction mechanisms from the literature and formed according to the SMAPE formula for preliminary estimations. Figure 2 presents the experimental measurements and the numerical data of three of the most accurate kinetic reaction mechanisms based on the SMAPE calculations that predicted the NO mole fractions closer to the experimental measurements at various equivalence ratios (0.6–1.4); see Figure 1.

The mole fraction of NO was taken at the end of the computational domain (at X = 2 cm), where the NO concentrations are defined under steady-state conditions while corresponding to the experimental emission sampling point of interest. Due to the estimation of the selected mechanisms, which present different trends when the equivalence ratio has changed from lean to rich conditions, analyses of the results will be divided into two categories, namely, lean to stoichiometric flames (ϕ = 0.6–1) and rich flames (ϕ = 1.2–1.4). In this way, the rationale behind obtaining different levels of NO formation/decomposition prediction by the mechanisms will be appropriately highlighted.

3.1. Lean Condition Flames

As shown in Figure 1, at ϕ = 0.6, most of the kinetic reaction mechanisms would not be able to estimate the mole fraction of NO properly and gave 100% as a percentage error. This number decreased severely when the equivalence ratio increased to 0.8 and 1, and then the estimation accuracy improved. The inefficient prediction of most kinetic reaction mechanisms at the very lean condition (ϕ = 0.6) is due to the instabilities of ammonia flames, causing difficulties in interpreting its chemical kinetics. Along with the lean conditions, many of the selected mechanisms gave a sharp variation with a high level of discrepancy compared to experimental measurements. In addition, when the equivalence ratio moves along the lean condition, most of the selected mechanisms' estimation fluctuates from low to high error values. Interestingly, along the lean range (0.6–1 of ϕ), both Glarborg [90] and Nakamura [69] mechanisms recorded low discrepancy values with errors ranging between 2–4%, respectively. Therefore, both mechanisms have been selected to study the characteristics of 70/30 vol% NH_3/H_2 flames at atmospheric conditions and along the lean stoichiometric range of ϕ, hence, comparing the outcomes of each mechanism to shed light on the reasons behind the discrepancies.

As shown in Figure 2, when ϕ is 0.6 to 1, the variation of estimated data obtained by Glarborg and Nakamura has the same trend as the measured data from experiments. Meanwhile, Wang's mechanism [46] has predicted those trends randomly. However, Wang's mechanism predicts NO mole fractions satisfactorily with a minor level of discrepancies at rich conditions, which will be explained later in the following section.

According to Figure 2, both the Glarborg and Nakamura kinetic models produced similar results when estimating the amount of H_2. The figure shows that the mole fraction of H_2 is at its lowest levels between 0.6 and 0.8 of ϕ. After this point, it gradually increases until reaching a high value at 1.4 of ϕ. This can be explained by the fact that a significant amount of H_2 is consumed in the post-flame zone for lean conditions of ϕ (0.6 and 0.8), but the mole fraction remains constant after passing through the flame zone at higher values of ϕ (1–1.4), indicating that it is not completely consumed in the post-flame zone (as shown in Figure 3).

Figure 4 shows that the kinetic reaction $NH_2 + H \rightleftharpoons NH + H_2$ (**R1**) significantly affects the formation of H_2, and its production rate increases sharply with increasing equivalence ratios. Additionally, both kinetic reactions $NH_3 + H \rightleftharpoons NH_2 + H_2$ (**R2**) and $NH + H \rightleftharpoons N + H_2$ (**R3**) positively promote H_2 production, demonstrating a considerable increase in the production rate at lean conditions. In addition, the kinetic reaction $HNO + H \rightleftharpoons NO + H_2$ (**R4**) shows opposite trends to what has been observed from the previous two reactions with a rate of production of H_2 governed by this kinetic reaction which decreases gradually with increasing equivalence ratio from 0.6 to 1. It is likely that due to the decrease in the level of HNO concentration, NO is also reduced.

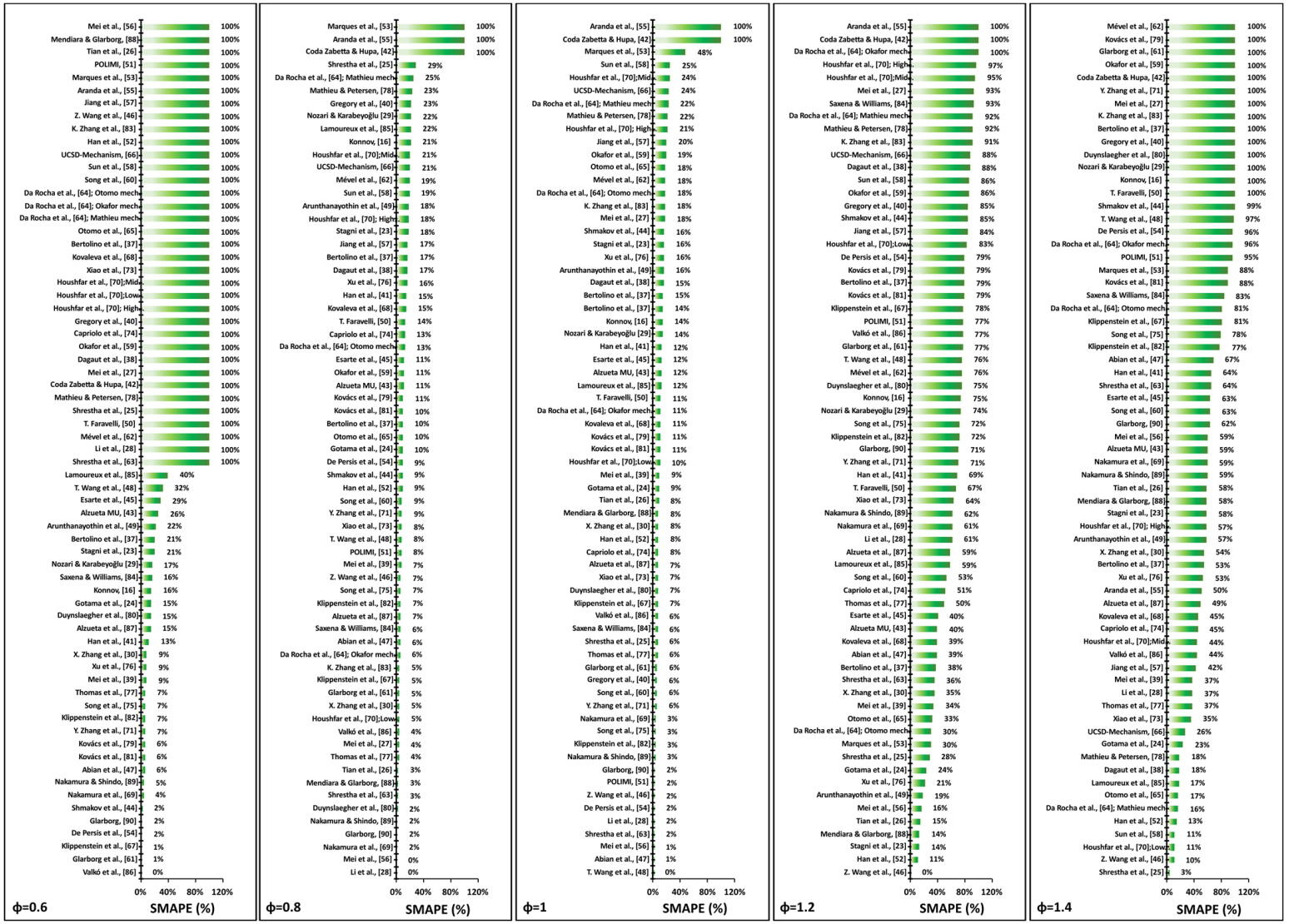

Figure 1. NO mole fractions for 67 reaction mechanisms calculated by symmetric mean absolute percentage error (SMAPE) formula at various equivalence ratios (ϕ).

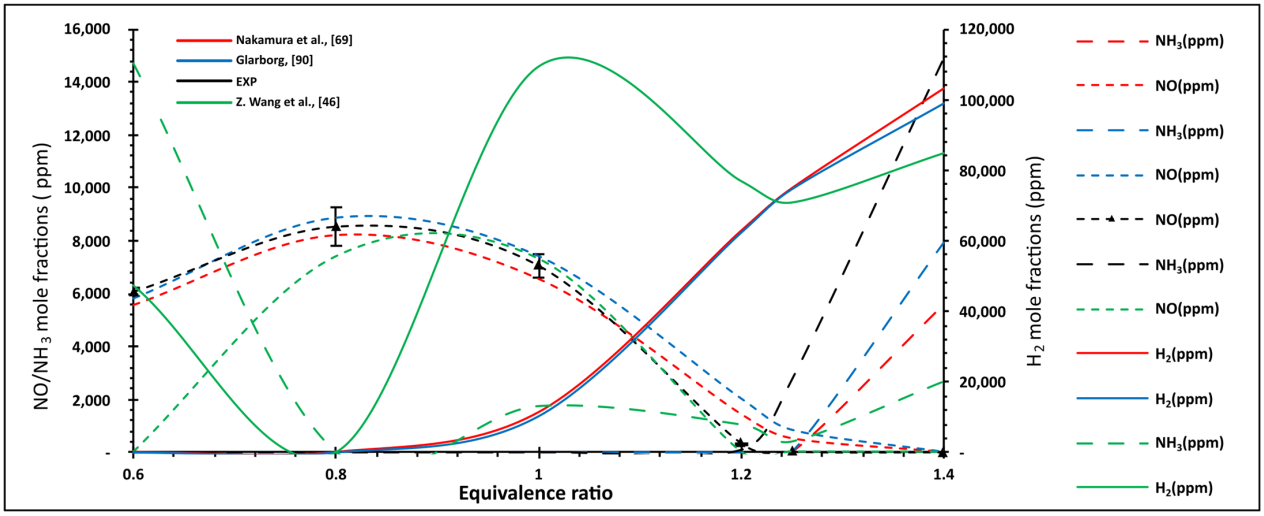

Figure 2. Variation of NO, NH_3, H_2 mole fractions as a function of equivalence ratio.

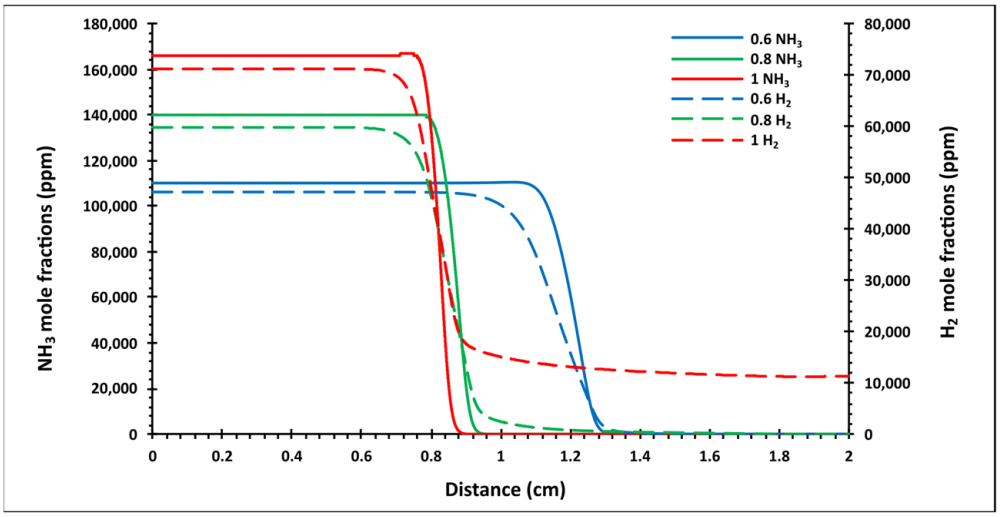

Figure 3. Variation of NH_3 and H_2 mole fractions as a function of axial distance at lean flame conditions (ϕ = 0.6, 0.8, 1) estimated by the Glarborg, [90] kinetic model.

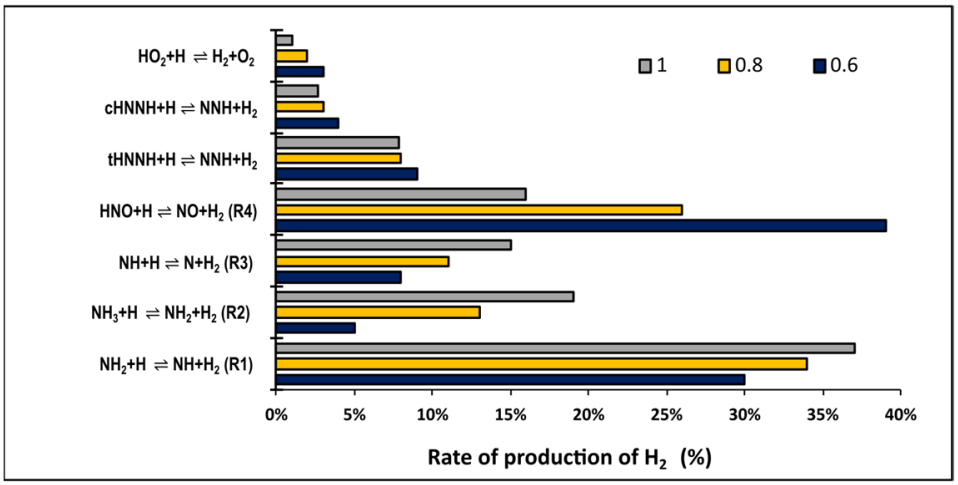

Figure 4. Rate of production analysis of H_2 in 70/30 vol% NH_3/H_2 premixed flame at lean conditions estimated by the Glarborg, [90] kinetic model.

Figure 2 also presents the variation of NO mole fraction as a function of equivalence ratio. The mole fraction of NO peaked at ϕ = 0.8. It has been noticed that the mole fraction of NO decreased gradually at either leaner or richer conditions than ϕ = 0.8. NO mole fractions estimated by Glarborg and Nakamura's kinetic models produced better performance compared to the other models considered here in the lean and close to stoichiometric zones. At ϕ = 0.6, the estimated NO value by Glarborg is identical to the experimental data. At the same time, Nakamura's prediction slightly underpredicts the NO mole fractions; see Figure 2. Concurrently, Wang's kinetic model predicted zero NO at very lean conditions. The Nakamura kinetic model demonstrates the same underestimation at 0.8 of ϕ, while the Glarborg mechanism showed overestimation by 4% compared to experimental measurements. The error estimation of Wang's model has improved from 100% at ϕ = 0.6 to 13% at ϕ = 0.8; see Figure 1. At the stoichiometric condition, Glarborg and Wang's model reaction gives nearly the same figures of NO mole fraction values, while the Nakamura model diverts slightly from the experimental result to give an underestimation trend of 7% SMAPE.

Sensitivity analyses have been performed at ϕ = 0.8 to highlight the reasons behind the discrepancies among the selected kinetic mechanisms, where NO concentration was the highest. Glarborg and Nakamura's mechanisms are selected for this analysis due to their better performance when compared to experimental results, as in Figure 2, giving minimum SMAPE among other tested mechanisms at lean conditions, as in Figure 1.

Figure 5 refers to the positive sensitivity coefficients of the kinetic reactions while demonstrating the most important kinetic reactions that promote the system reactivity and increase the mole fraction of NO. The positive sensitivity coefficients are normalized to their sum separately and shown as a percentage. Both kinetic models of Glarborg and Nakamura have displayed high positive sensitivity toward the chain branching reaction $H + O_2 \rightleftharpoons O + OH$ (**R5**). This reaction promotes the system's reactivity by producing more reactive OH radicals. Even though the Nakamura mechanism has a higher sensitivity coefficient of the kinetic reaction R5 than Glarborg, both kinetic models gave nearly the same sensitivity coefficient of the reaction $NH + OH \rightleftharpoons HNO + H$ (**R6**), which in turn increases HNO pools to promote NO formation. In Nakamura's mechanism, the kinetic reactions $N_2O + O \rightleftharpoons 2NO$ (**R7**), $NO + HO_2 \rightleftharpoons NO_2 + OH$ (**R8**), $HNO + O \rightleftharpoons NO + OH$ (**R9**), $NH + O_2 \rightleftharpoons HNO + O$ (**R10**), $N + OH \rightleftharpoons NO + H$ (**R11**), $H_2 + OH \rightleftharpoons H + H_2O$ (**R12**), and $HNO + OH \rightleftharpoons NO + H_2O$ (**R13**) have sensitivity coefficients in the range of 3–15%, but their sensitivity coefficients are equal to zero in Glarborg's mechanism. Similarly, Glarborg's mechanism shows the reactions reactivity of $NH_2 + O \rightleftharpoons HNO + H$ (**R14**), $2NH_2$ $(+M \rightleftharpoons N_2H_4(+M)$ (**R15**), R6, $NH_2 + HO_2 \rightleftharpoons NH_3 + O_2$ (**R16**), $NH_2 + NH \rightleftharpoons tHNNH + H$ (**R17**), R12, and R1 in the range of 3–16%; however, they do not show any sensitivity toward promoting NO mole fraction in Nakamura's mechanism.

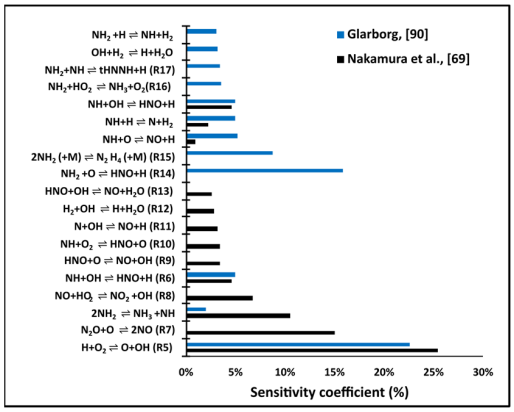

Figure 5. Reactions with the largest positive local sensitivity coefficient for NO in 70/30 vol% NH_3/H_2 premixed flame at ϕ = 0.8 estimated by the Glarborg, [90] and Nakamura et al., [69] kinetic models.

Figure 6 presents the reactions with negative sensitivity towards NO production. The negative sensitivity coefficients are normalized to their sum separately and shown as a percentage. As shown in Figure 6, Glarborg's mechanism shows high negative sensitivity coefficients for the kinetic reactions '$NH_2 + NO \rightleftharpoons N_2 + H_2O$ (**R18**)' and $NH_2 + NO \rightleftharpoons NNH + OH$ (**R19**). In contrast, for Nakamura's mechanism, the same kinetic reactions demonstrate 4% and 1% negative sensitivities, respectively. Both reactions consume the important key radical (NH_2), destroying NO to form N_2 and NNH. Additionally, the sensitivity coefficient of the reaction $NH + NO \rightleftharpoons N_2O + H$ (**R20**) has a higher effect in Nakamura's model (12%) than in Glarborg's, where it is estimated at 5%. In both mechanisms, the latter reaction impedes the system reactivity by producing less reactive H radicals. In addition, Nakamura's kinetic model shows how 8 of the kinetic reactions hinder the reactivity of the NO mole fraction. Those kinetic reactions do not influence the system reactivity in Glarborg's mechanism; see Figure 6.

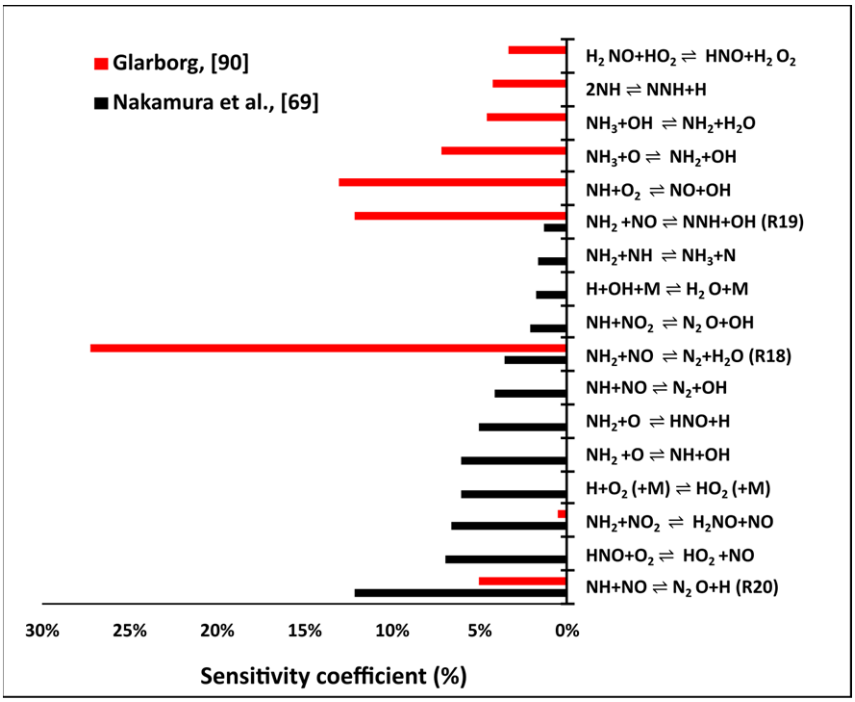

Figure 6. Reactions with the largest negative sensitivity coefficients for NO in 70/30 vol% NH_3/H_2 premixed flame at ϕ = 0.8 estimated by the Glarborg, [90] and Nakamura et al., [69] kinetic models.

The present study has also considered the ROP analysis of NO to shed light on the most important kinetic reactions contributing to NO formation/consumption. Figures 7–9 outline the variation of the key reactions of NO production/decomposition along the axial axis of the computational domain in terms of equivalence ratio. The figures have been established based on Nakamura kinetic model's estimation. The spatial distribution of the key reactions with the maximum mole fraction of NO formation/decomposition has been selected for each equivalence ratio using the mechanism chosen to highlight the variation of the reactions.

As can be seen from Figure 7, the total mole fraction of NO decreased at first and then increased downstream along the lean range of equivalence ratios. The declining pattern in NO formation is due to the high reactivity of R18, R19, and R20 in the reduction of NO mole fraction. Besides all the mentioned reactions having the most significant consuming effect of NO, the former reactions' consumption rate (R18) decreases when the equivalence ratio increases from 0.6 to 1. At the same time, the reaction (R20) demonstrates a climbing trend with an increasing equivalence ratio; see Figure 8. Furthermore, the kinetic reaction $N_2 + O \rightleftharpoons N + NO$ (**R21**) substantially impacts the NO decomposition rate at lean conditions

when the temperature of the reaction increase as a function of the equivalence ratio. This is because the kinetic reaction R21 is one of the thermal NO reactions governed by high temperature; hence, it is listed under the Zeldovich mechanism [65], as in Figures 7 and 8. In addition, NH + NO ⇌ N_2 + OH (**R22**) also demonstrates an increasing trend with an equivalence ratio, and its reactivity peaks at stoichiometry due to the increase in NH radicals availability; see Figures 8 and 10.

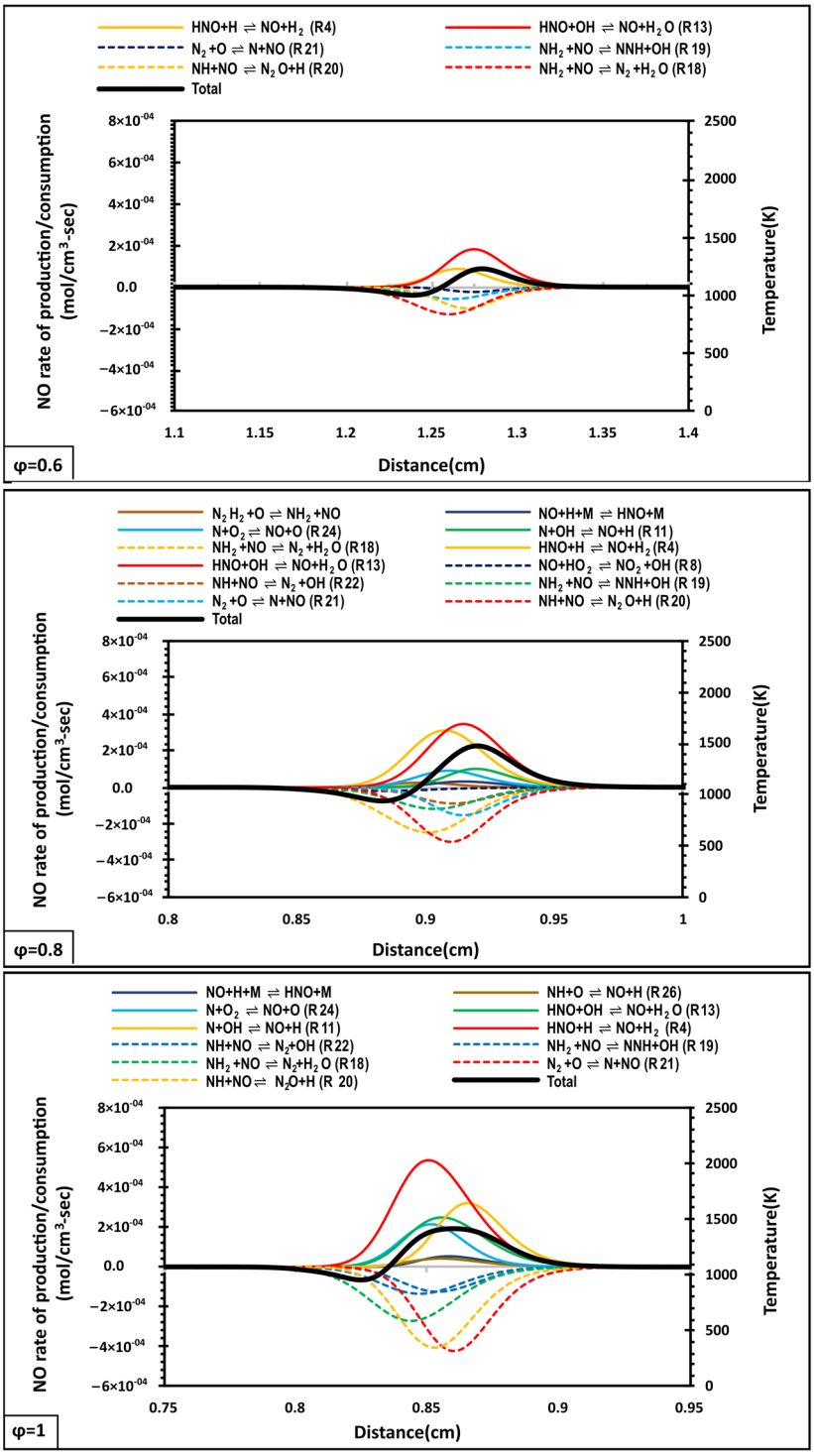

Figure 7. The rate of production/consumption of NO in 70/30 (vol%) NH_3/H_2 mixture at lean conditions estimated by the Nakamura et al., [69] kinetic model.

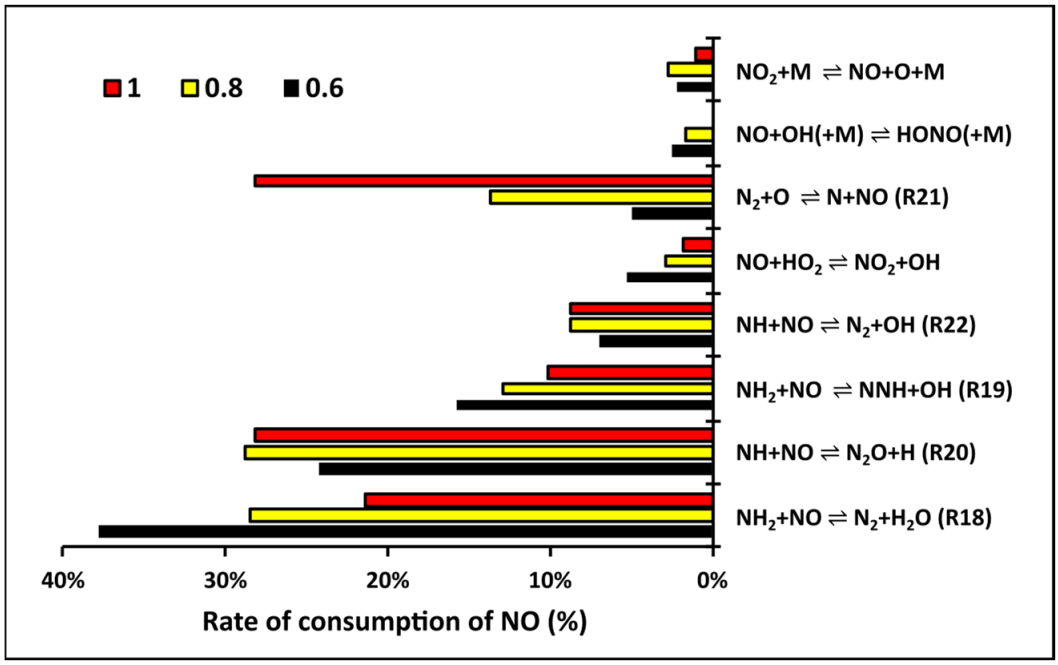

Figure 8. Rate of consumption (in %) as a function of equivalence ratio estimated by the Nakamura et al., [69] kinetic model.

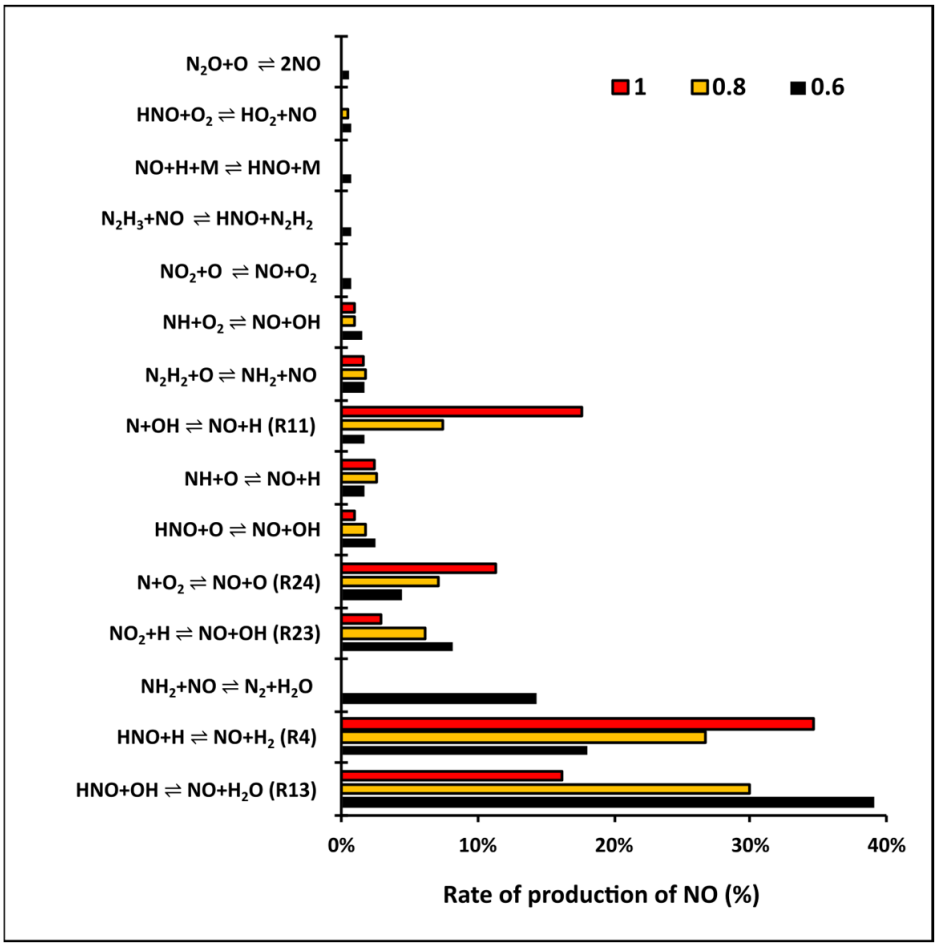

Figure 9. Rate of production (in %) as a function of equivalence ratio estimated by the Nakamura et al., [69] kinetic model.

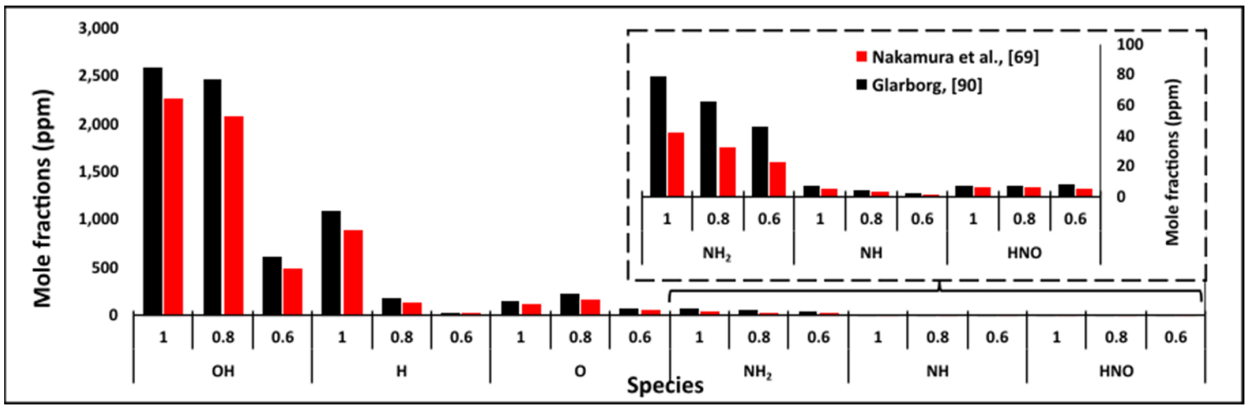

Figure 10. Varieties of mole fractions of OH, H, O, NH_2, NH, HNO as a function of equivalence ratio estimated by two selected kinetic models.

The NO mole fraction increases significantly downstream due to the high reactivity of the reactions R13 and R4, which demonstrate a dominant effect in the formation of NO, as well as the contribution from the reactions $NO_2 + H \rightleftharpoons NO + OH$ (**R23**), $N + O_2 \rightleftharpoons NO + O$ (**R24**), and R11. The thermal reactions R24 and R11 hardly take part in the formation of NO, especially at $\phi = 0.6$, due to the temperature dependency of these reactions. As a result, they show a rapid response to NO formation when the equivalence ratio increases to the stoichiometric condition where the temperature is the highest; see Figures 7 and 9. The NO production rate from the reaction R13 reaches the maximum at $\phi = 0.6$ and then decreases as ϕ increases, even though the OH radical availability increases; see Figure 10. R4 shows the opposite trend, where the NO production rate is directly proportional to ϕ; see Figure 9.

To justify the opposite behavior of the latter kinetic reactions (R4 and R13) in promoting NO formation, Table 2 lists the key reactions of NO production and shows that the kinetic reaction 'R13' has a more remarkable pre-exponential factor (A) than that of R4. Both reactions are sensitive to the temperature, but the kinetic reaction 'R4' is more sensitive, and its reactivity increases more rapidly with temperature than reaction R13. Additionally, the abundance of H radicals improves the R4 reactivity to become more dominant at stoichiometry, compared to the reaction R13; see Figures 9 and 10. The kinetic formation process of NO is mainly governed by HNO, NH, N, and NO_2 mole fractions, and then it is consumed early by the $DeNO_x$ process through the action of NH_2, NH, and N radicals at the reaction zone; see Figure 11.

Table 2. Key reactions of NO formation generated from Nakamura's kinetic model. Units are mol, cm, s, cal.

NO.	Reaction	Glarborg, [90]			Nakamura et al., [69]		
		A	n	E	A	n	E
R13	$HNO + OH \rightleftharpoons NO + H_2O$	6.3×10^{10}	0.390	3782	3.6×10^{13}	0.00	0
R4	$HNO + H \rightleftharpoons NO + H_2$	6.6×10^{10}	0.940	495	4.4×10^{11}	0.72	650

Glarborg's mechanism shows the same NO formation/consumption trend as Nakamura's kinetic model. The NO formation rate through the reactions of HNO radicals is considerably higher than the NO consumption rate via NH_2 and NH radicals. Therefore, the total rate of NO is increased downstream due to the high promotion of NO mole fraction; see Figure 12. Additionally, the kinetic reactions of R4, $NH + O \rightleftharpoons NO + H$ (**R25**), and R9, as well as the thermal NO reactions (R24 and R11), contribute towards the increasing NO formation rate; see Figures 13 and 14. On the other hand, the chain-termination reaction 'R18', chain-branching reaction 'R19', R20, and the temperature-dependent reaction 'N +

NO ⇌ N2 + O (**R26**)' in Nakamura's kinetic model are the dominant kinetic reactions in the consumption of NO; Figures 12 and 13.

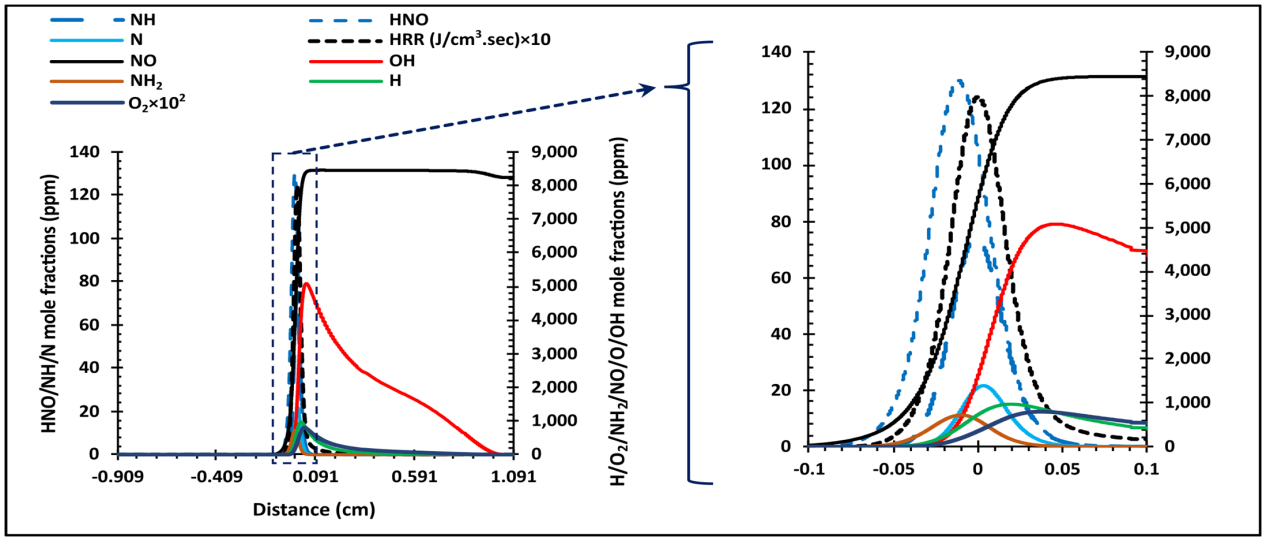

Figure 11. Variation of mole fractions of N, NH, NH_2, NO, OH, H, and HNO and heat release rate (HRR) in flame structure estimated by the Nakamura et al., [69] mechanism at ϕ = 0.8.

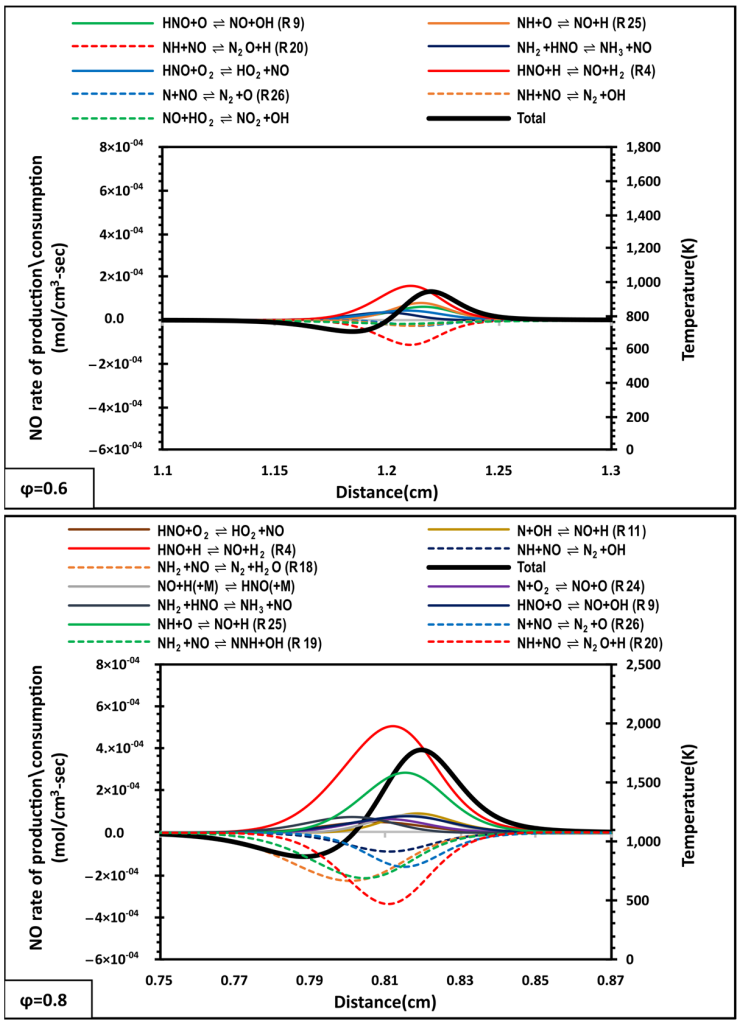

Figure 12. *Cont.*

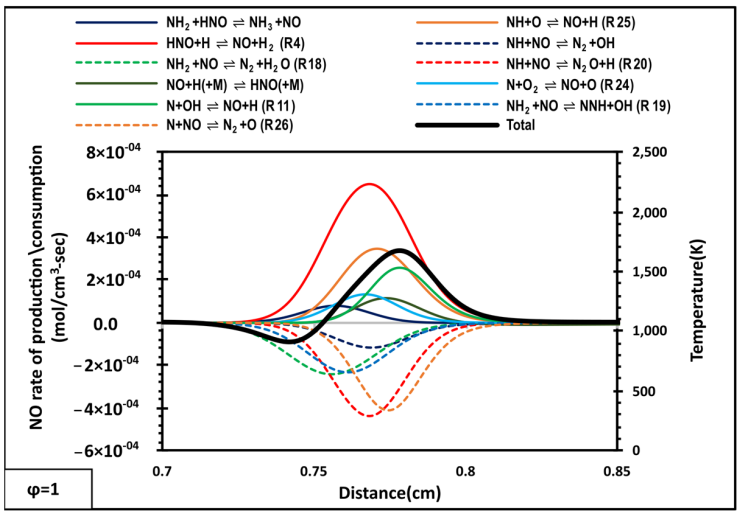

Figure 12. The rate of production/consumption of NO in 70/30 (vol%) NH_3/H_2 mixture at lean conditions estimated by the Glarborg, [90] kinetic model.

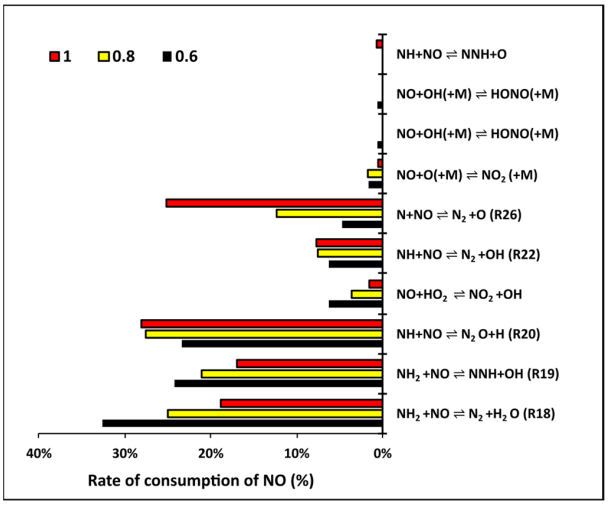

Figure 13. Rate of consumption (in %) as a function of equivalence ratio estimated by the Glarborg, [90] kinetic model.

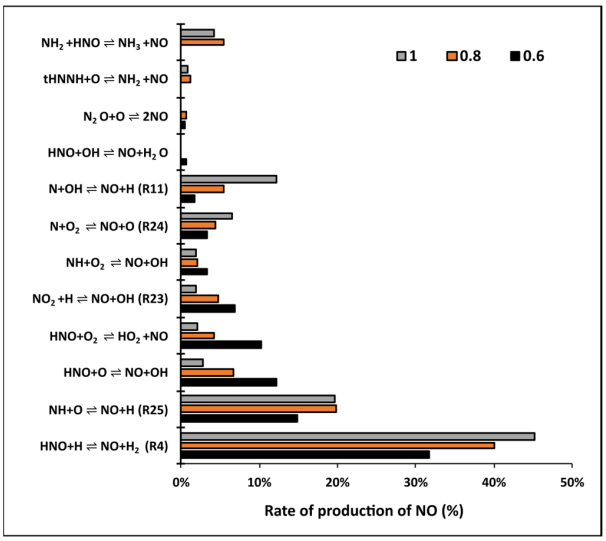

Figure 14. Rate of production (in %) as a function of equivalence ratio estimated by the Glarborg, [90] kinetic model.

Figure 15 shows the kinetic schemes predicted by the best-performing models. It illustrates the chemical reaction pathways of NO formation/decomposition and the net reaction rate of the kinetic reactions that influence NO mole fractions. It also demonstrates the tendency of the radical's percentage (%) reactivity toward either formation or decomposition of NO. Reaction pathway analyses were conducted at equivalence ratios that yield the highest NO formation (ϕ = 0.8) and at a temperature of 1770 K, which corresponds to the point of maximum occurrence of the total NO component; see Figure 12. As shown in Figure 15, the kinetic mechanisms of Glarborg and Nakamura show that HNO, NH, and N radicals form the main pathways for NO formation. At the same time, N, NH, and NH_2 are responsible for consuming the majority of NO. The kinetic scheme of Glarborg demonstrates the substantial contribution of the HNO $\rightarrow$ NO pathway (65%) towards NO formation through the reaction R4. On the other side, N, NH, and NH_2 radicals tend to consume NO at different concentrations and produce N_2 through the kinetic reactions R26, R20, R22, R18, and R19, where activities of N, NH_2, and NH radicals are 53%, 25%, and 22%, respectively, while 96% of NH_2 is consumed via the reaction R19 to convert NO to NNH. Even though the kinetic models display similar NO production/destruction patterns, the concentration of the reactions varies from one kinetic model to another.

Regarding the description of NO chemistry, the kinetic models of Glarborg and Nakamura demonstrate the same NO formation pathways at a temperature of 1770 K. Both tested models show the NO formation chemistry through the same pathways described by the following sequences: $NH_3 \rightarrow NH_2 \rightarrow NH \rightarrow N \rightarrow NO$, $NH_3 \rightarrow NH_2 \rightarrow NH \rightarrow HNO \rightarrow NO$, $NH_3 \rightarrow NH_2 \rightarrow NH \rightarrow NO$, and $NH_3 \rightarrow NH_2 \rightarrow HNO \rightarrow NO$. The kinetic schemes of Glarborg and Nakamura reveal another reason behind the differences in the estimation among selected kinetic models. The reactive radicals (H, OH, and O) that participate in the formation of NO through their interaction with HNO, NH, and N demonstrate different percentages of radicals' abundance in both mechanisms; see Figure 15.

Figures 16 and 17 demonstrate the most important reactions that take part in promoting/consuming NO, respectively. As shown in Figure 16, the kinetic reaction R13 plays a significant role in NO formation in Nakamura's mechanism, especially at ϕ = 0.6, but contributes only 1% in NO formation in Glarborg's kinetic model. The reason can be justified by the effect of the Arrhenius parameters that govern the reaction, especially the activation energy. As seen in Table 2, the activation energy of reaction R13 is set to 0 in Nakamura's model. The reaction here is independent of temperature compared to its effect on Glarborg's mechanism, identified as a temperature-dependent reaction. An absence in the contribution of the latter reaction in the formation of NO when ϕ equals 0.8 and 1 in Glarborg's mechanism has also bee noticed. Further, the NO production rate for the kinetic reactions R4, R9, R25, and HNO + $O_2 \rightleftharpoons HO_2$ + NO (**R27**) is higher in Glarborg's kinetic model compared to Nakamura's at lean conditions. The figures for the consumption rate are illustrated in Figure 17, where predictions by both kinetic models show nearly the same level of estimation. Despite some kinetic reactions demonstrating a slight increase in the estimation by Glarborg's mechanism, the variations between the kinetic reactions by both mechanisms are still narrow and not substantial compared to those of Figure 16.

The overprediction in the formation of NO by Glarborg's mechanism is also due to the high heat release rate (HRR). Figures 11 and 18 illustrate the variation of mole fractions of key species responsible for the formation/consumption of NO. It has been noticed that the heat release rate calculated by Glarborg's mechanism is higher than that estimated by Nakamura's model. Since increasing the heat release rate will improve the system reactivity and boost the speed of the reaction, according to Chen et al. [1], both NH_2 and OH radicals can be considered as criteria/markers for the growth of HRR.

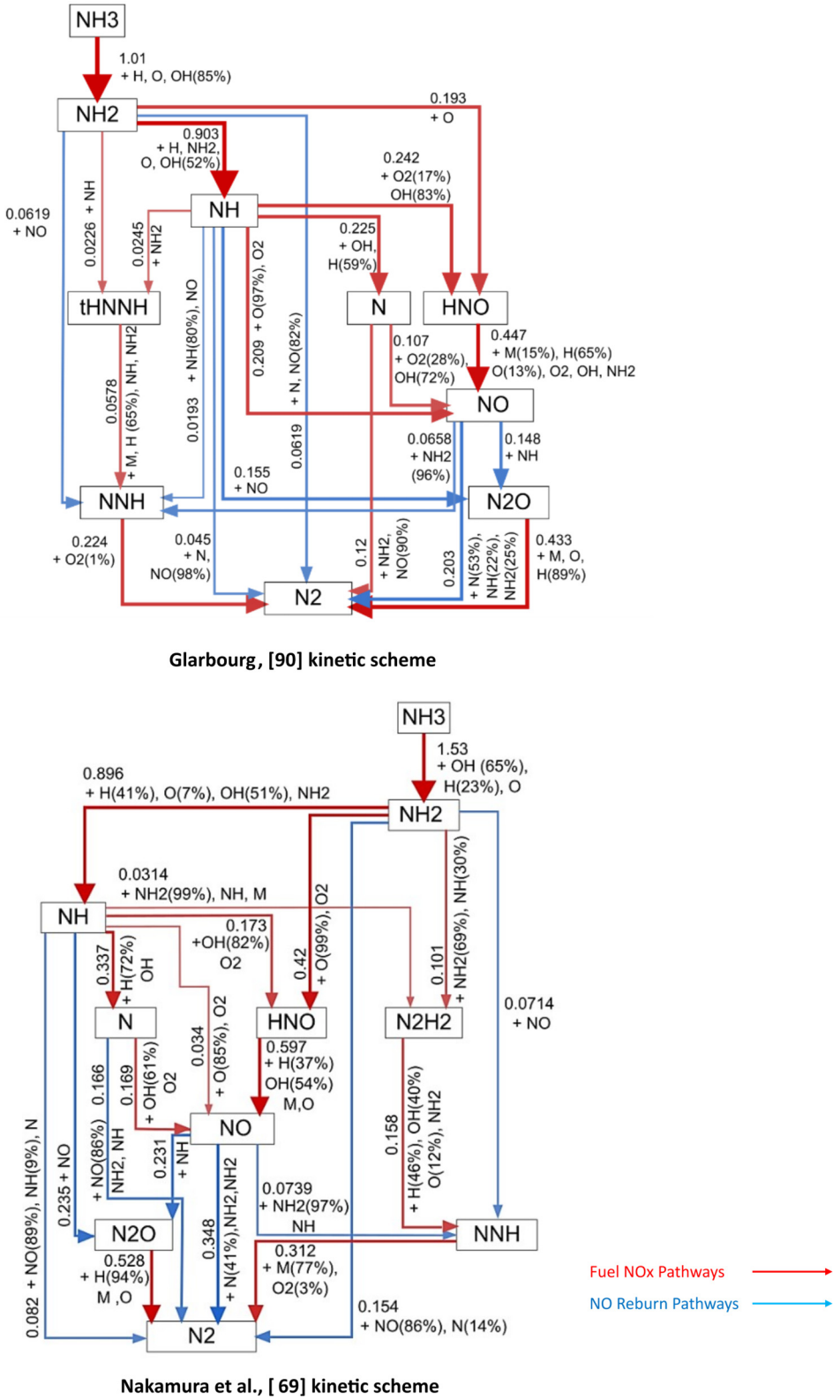

Figure 15. Chemical reaction pathways of NO formation/consumption at flame zone (T = 1770 K) and at ϕ = 0.8 predicted by the Glarborg, [90] and Nakamura et al., [69] kinetic models. Arrow lines refer to chemical transformations, percentages (%) show the contribution of a reactant to the transformation, numbers stand for the net reaction rate in kmol/m^{3}s, which is also visualized by line thickness.

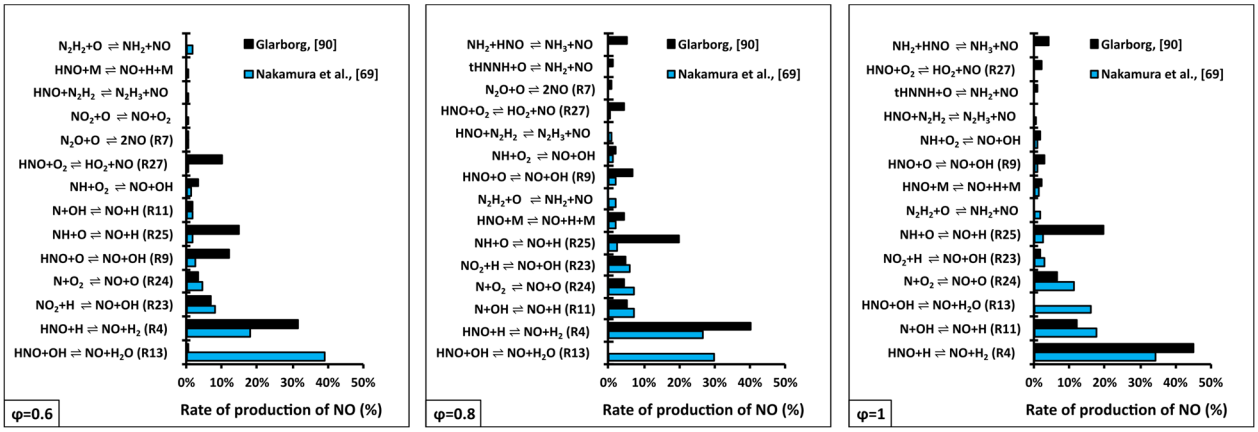

Figure 16. Rate of production (in %) of NO mole fractions at lean conditions estimated by the Nakamura et al., [69] and Glarborg, [90] kinetic models.

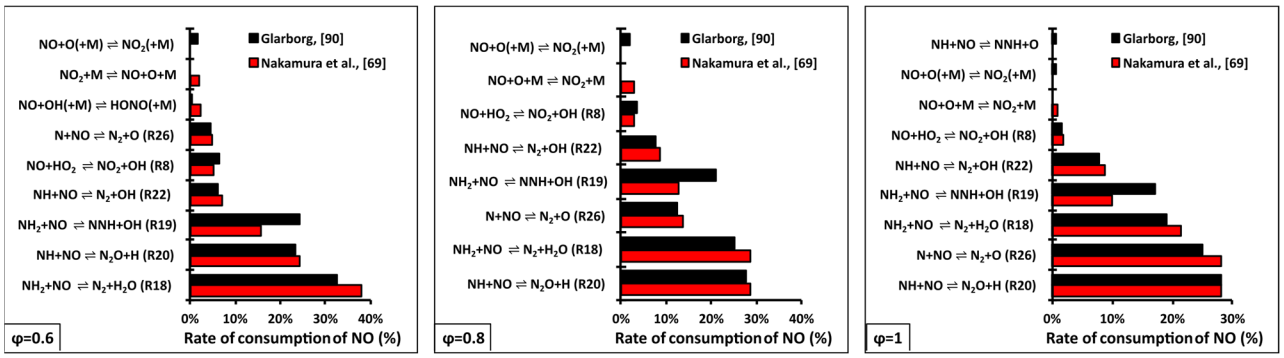

Figure 17. Rate of consumption (in %) of NO mole fractions at lean conditions estimated by the Nakamura et al., [69] and Glarborg, [90] kinetic models.

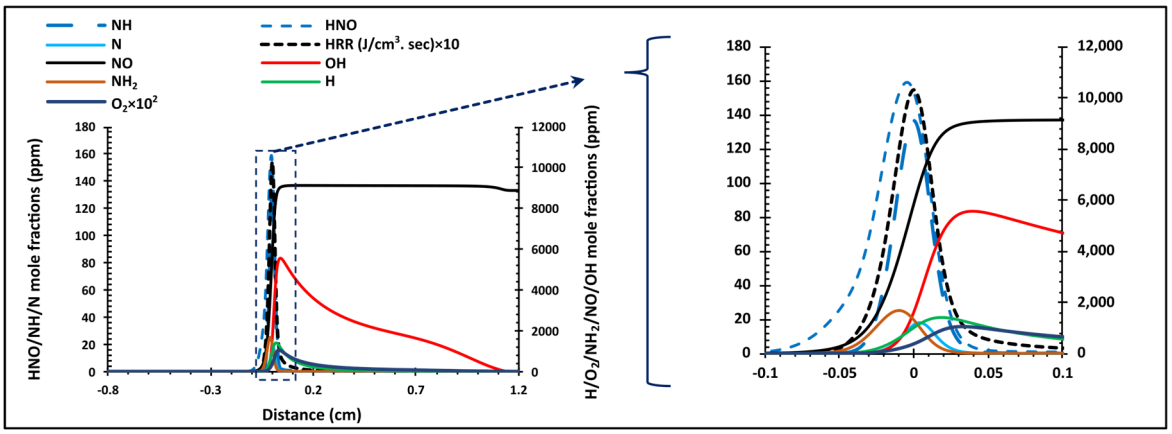

Figure 18. Variation of mole fractions of N, NH, NH_2, NO, OH, H, and HNO and heat release rate (HRR) in flame structure estimated by the Glarborg, [90] mechanism at ϕ = 0.8.

3.2. Rich Condition Flames

Most tested kinetic models gave a high estimation error based on SMAPE at ϕ = 1.2; see Figure 1. Both Nakamura and Glarborg kinetic models recorded 100% SMAPE, indicating a very high level of discrepancies compared to the experimental results. The kinetic reaction mechanism of Wang [46] has displayed excellent estimation of NO mole fraction among other investigated mechanisms; see Figures 1 and 2. The prediction of Wang's mechanism obtained 0% SMAPE at ϕ = 1.2 and 10% at ϕ = 1.4. Therefore, the kinetic mechanism of Wang has been selected to analyze the chemical kinetic behavior of the reactions under rich

conditions. Further, due to the deterioration in the performance of Nakamura's mechanism at rich conditions, especially when ϕ = 1.2, the Nakamura mechanism will also be compared to Wang's outcomes to investigate the reasons behind the discrepancy in NO mole fractions at rich conditions.

Figures 19 and 20 show the reactions with the largest positive and the negative sensitivity coefficients for NO mole fractions in the Nakamura and Wang's kinetic models at ϕ = 1.2. The positive and negative sensitivity coefficients are normalized to their sum separately and shown as a percentage. Figure 19 highlights the kinetic reactions with the most significant sensitivity coefficients in percentage (%) and indicates a positive influence towards the promotion of NO mole fraction. It should be noted that most kinetic reactions promote the reactivity of the system by producing either more reactive OH, H, O, or HO_2 radicals, such as the chain branching reactions R5, $H_2 + O \rightleftharpoons H + OH$ (**R28**), R12, and $H_2 + M \rightleftharpoons 2H + M$ (**R29**). To show the differences in the prediction among the selected mechanisms, Figure 19 indicates that Wang's kinetic model shows a slight increase in reactivity for the kinetic reactions R28, R12, $O + H + M \rightleftharpoons OH + M$ (**R30**), and $H + OH + M \rightleftharpoons H_2O + M$ (**R31**). Along with that, Wang's mechanism also demonstrates a higher value of estimation for the reaction R5 and a lower value for R29 compared to Nakamura's model, which, in turn, shows the opposite trend for Wang's model in the estimation of sensitivity coefficients of the reactions mentioned above. The reason behind the variation of the sensitivity values of the kinetic reactions R5 and R29 among the mentioned mechanisms can be attributed to the difference in Arrhenius parameters that governed the rate of reaction for each kinetic reaction, and their values differ among the selected mechanisms; see Table 3.

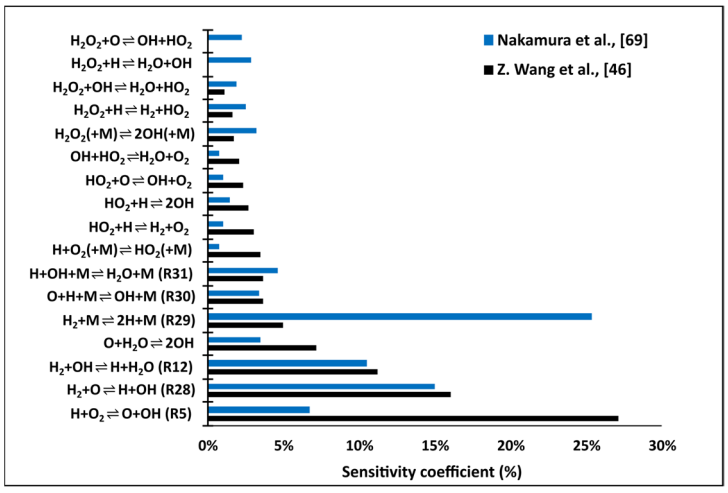

Figure 19. Reactions with the largest positive local sensitivity coefficient for NO in 70/30 (vol%) NH_3/H_2 premixed flame at ϕ = 1.2 estimated by the Nakamura et al., [69] and Z. Wang et al., [46] kinetic models.

Figure 20 shows sensitivity analyses of kinetic reactions with negative coefficients in percentage (%) and illustrates the tendency of the reactions towards impeding NO production. Both models demonstrate different kinetic reactions controlling the retardation of NO production. The results only share three kinetic reactions with different values, namely, $N_2H_2 + NH_2 \rightleftharpoons NH_3 + NNH$ (**R32**), R4, and R24. Even though the kinetic reaction R32 has the same Arrhenius parameters listed in both selected models, Table 3, the negative value of the activation energy tends to decrease the reactivity of the kinetic reaction when the system's temperature increases. As Nakamura's mechanism has higher temperature estimation than Wang's model, this can be attributed to the high estimation value of the latter reaction by Wang's mechanism rather than Nakamura's model; see Figure 21. Further, the reaction rate of the other kinetic reactions, R4 and R24, increases with temperature. The former reaction (R4) also has the same values of Arrhenius parameters in both tested

models, but its reaction rate estimated by the Nakamura's kinetic model is higher than that of Wang's mechanism due to the high-temperature estimation by Nakamura's mechanism.

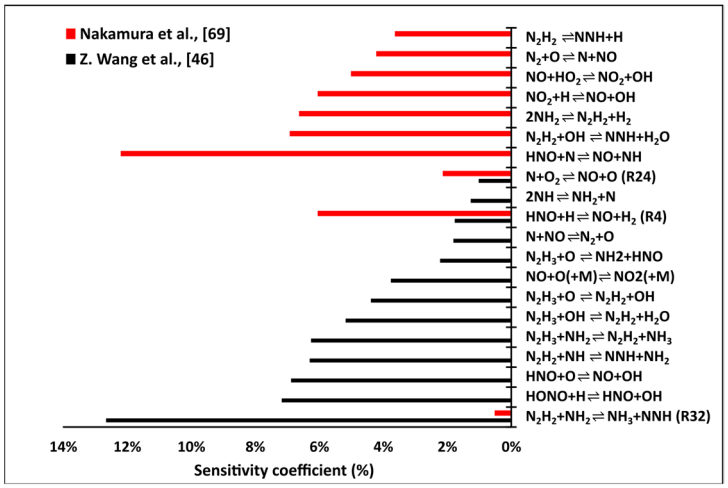

Figure 20. Reactions with the largest negative sensitivity coefficients for NO in 70/30 (vol%) NH_3/H_2 premixed flame at ϕ = 1.2 estimated by the Nakamura et al., [69] and Z. Wang et al., [46] kinetic models.

Table 3. Key reactions influencing NO formation/consumption of NH_3-H_2 flames at rich conditions and for two kinetic mechanisms. Units are mol, cm, s, cal.

NO.	Reaction	Z. Wang et al., [46]			Nakamura et al., [69]		
		A	n	E	A	n	E
1	$H + O_2 \rightleftharpoons O + OH$ (R5)	5.0712×10^{15}	−0.48596	16126.7	1.040×10^{14}	0	15,286.0
2	$H_2 + M \rightleftharpoons 2H + M$ (R29)	4.9806×10^{18}	−1.21273	612.04	4.577×10^{19}	−1.4000	104,400.0
3	$N_2H_2 + NH_2 \rightleftharpoons NH_3 + NNH$	8.8×10^{-2}	4.05	−1610	8.8×10^{-2}	4.05	−1610.0
4	$HNO + H \rightleftharpoons NO + H_2$	4.4×10^{11}	0.72	650	4.4×10^{11}	0.7200	650.0
5	$N + O_2 \rightleftharpoons NO + O$	5.9×10^{9}	1	6280	6.4×10^{9}	1	6280.0
6	$N + OH \rightleftharpoons H + NO$	2.17×10^{14}	0	49,500	3.800×10^{13}	0	0
7	$NH + O \rightleftharpoons NO + H$	9.9×10^{14}	−0.1	69,900	2.000×10^{13}	0	0
8	$HNO + OH \rightleftharpoons NO + H_2O$	3.600×10^{13}	0	0	3.600×10^{13}	0	0
9	$N + NO \rightleftharpoons N_2 + O$	1.529×10^{13}	−0.0027	−185.41	1.000×10^{14}	0	75,490.0
10	$NH + NO \rightleftharpoons N_2 + OH$	2.7×10^{12}	−0.0721	−512	2.200×10^{13}	−0.23	0

Figures 22 and 23 present the variation of the rate of production/consumption of NO estimated by Wang and Nakamura's kinetic mechanisms, respectively, at rich conditions and indicate the spatial distribution of the most important kinetic reactions in the formation/consumption of NO. The total component of NO starts to decrease to a negative value at the earlier stage of the reaction zone due to the action of R18, R19, and R20, which are responsible for NO consumption due to the high reactivity of the NH_2 and NH radicals. The total NO formation then increases due to the positive effects of the kinetic reactions R4, R25, R13, R11, and $NH_2 + HNO \rightleftharpoons NH_3 + NO$ (**R33**), where the kinetic reaction 'R4' has the highest reactivity among the other kinetic reactions. The total component of NO decreased afterward due to the thermal NO reactions of Zeldovich mechanism R26 and R22', as well as the reaction $NH + NO \rightleftharpoons NNH + O$ (**R34**) in lowering the mole fraction of NO downstream by consuming it via the high reactivity of N, and NH radicals. Most importantly, the amplitude of the total NO formation decreases when the equivalence ratio increases from 1.2 to 1.4. This effect leads to a rate of consumption that is more than the NO production rate, which, in turn, lowers the mole fraction of NO; see Figures 24 and 25.

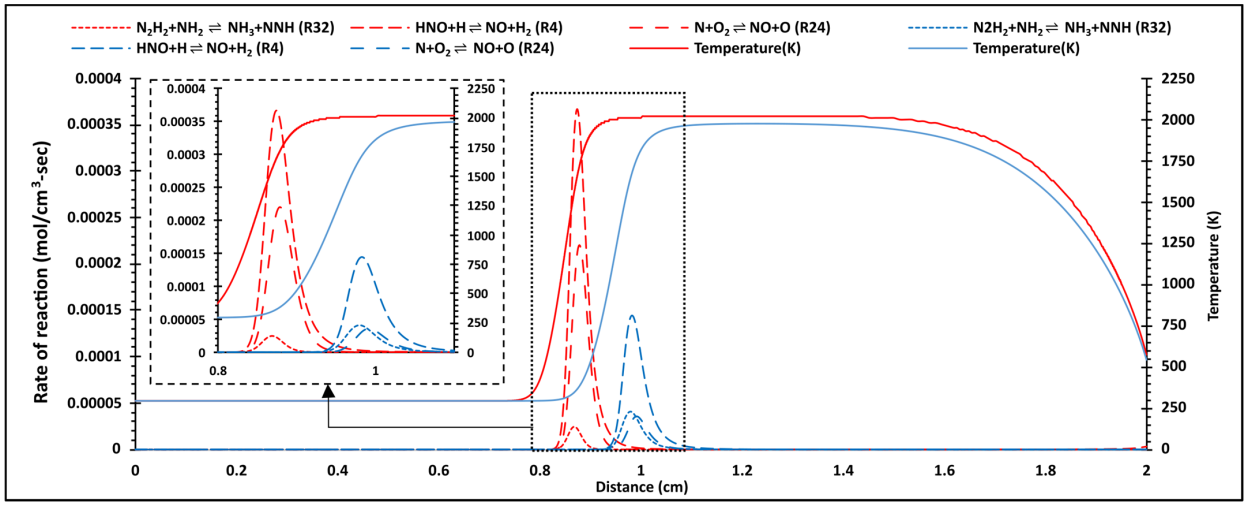

Figure 21. The reaction rate profiles of reactions most influential to the formation/reduction of NO mole fractions for 70/30 vol% NH_3/H_2 mixture at ϕ = 1.2; The result for the Nakamura et al., [69] and Z. Wang et al., [46] models are shown with red and blue lines, respectively.

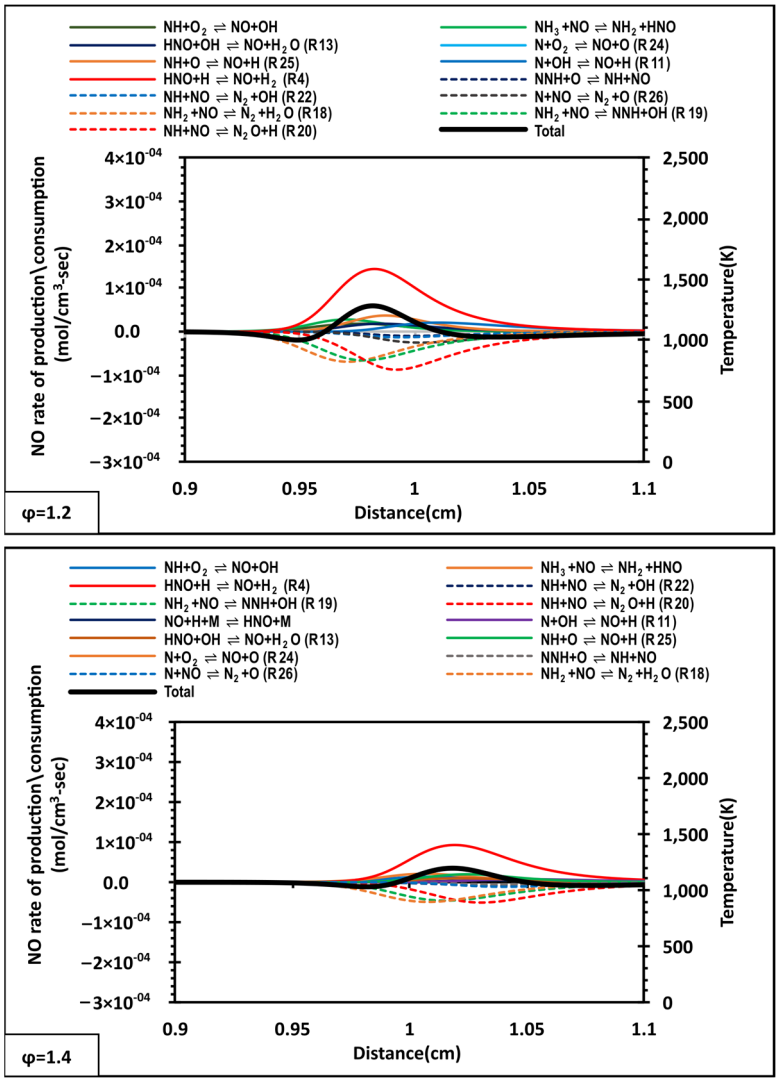

Figure 22. The rate of production/consumption of NO in 70/30 (vol%) NH_3/H_2 mixture at rich conditions estimated by the Z. Wang et al., [46] model reaction.

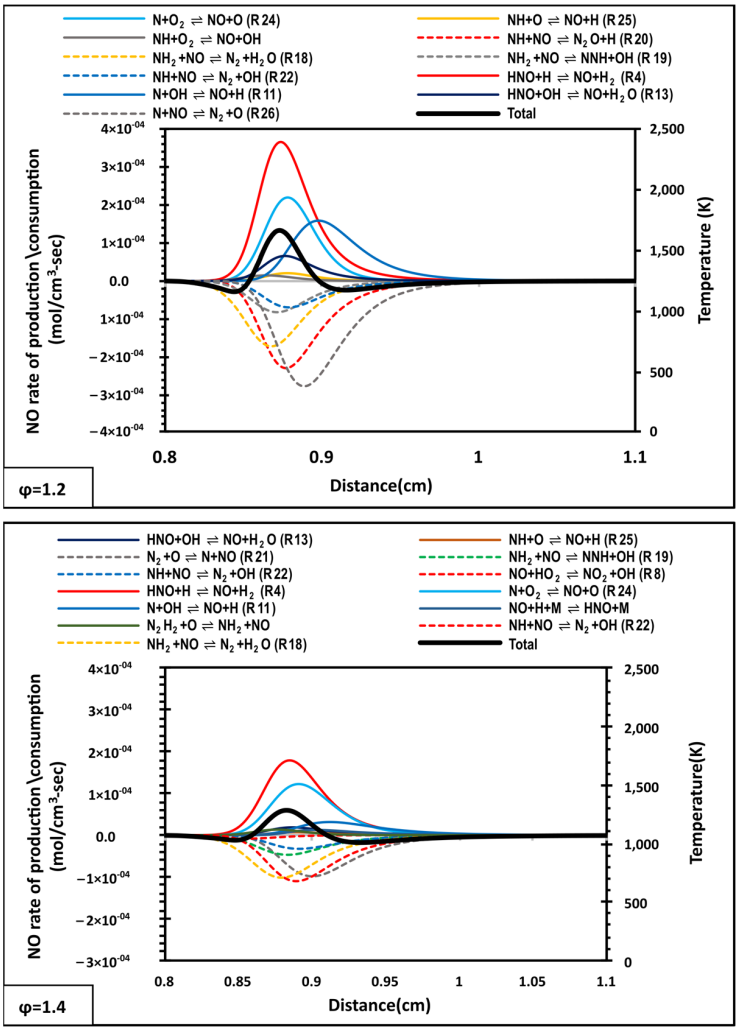

Figure 23. The rate of production/consumption of NO in 70/30 (vol%) NH_3/H_2 mixture at rich conditions estimated by the Nakamura et al., [69] model reaction.

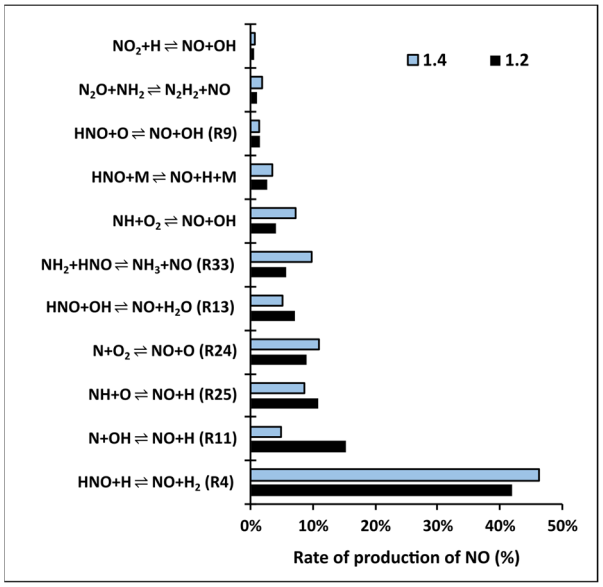

Figure 24. Rate of production figures in (%) as a function of equivalence ratio estimated by the Z. Wang et al., [46] kinetic model.

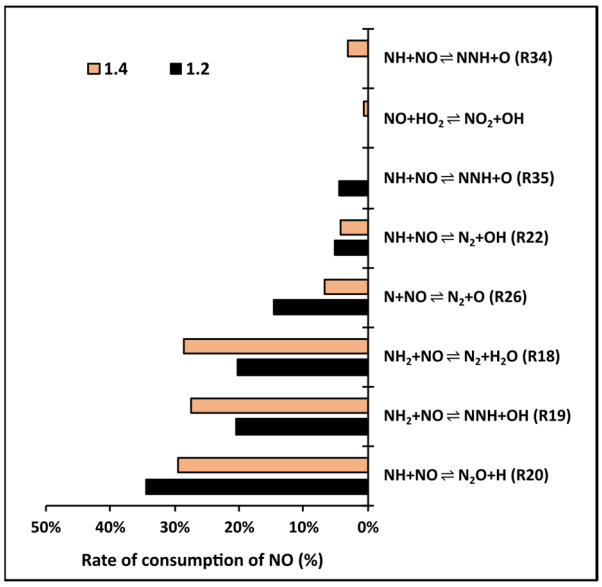

Figure 25. Rate of consumption figures in (%) as a function of equivalence ratio estimated by the Z. Wang et al., [46] kinetic model.

Figure 26 illustrates the kinetic schemes for the best-performing kinetic models, which present the chemical kinetic pathways of the kinetic reactions taking part in the formation/consumption of NO at the reaction zone when the system's temperature is equal to 1513 K at ϕ = 1.2. The target temperature of 1513 K was selected based on the optimal point of total NO component occurrence, as observed in Figure 23. The temperature was chosen as it corresponded to the maximum yield of the NO component, thereby enabling a more comprehensive analysis of the reaction pathways. As shown in Figure 26, both Wang and Nakamura's kinetic models demonstrate the HNO $\rightarrow$ NO pathway, which still plays a substantial role at rich conditions in the consumption of HNO and produces NO. The kinetic scheme pathways of Wang mechanisms demonstrate the tendency of high reactive H radical (68%) with HNO through the reaction R4, followed by NH_2 with 17% via R33. Most importantly, the net reaction rate of the former reaction (R4) decreased to nearly half of its value compared to the same reaction at lean conditions. For reducing NO, NH_2 radicals show a high intensity of reactivity of 96% in consuming NO to produce NNH radicals. The net reaction rate of the latter reaction increased by 0.084 kmol/m^3s compared to the value of the same reaction in lean conditions. In addition, the NO $\rightarrow$ N_2 pathway has a substantial role in NO consumption, with 0.107 kmol/m^3s compared to other consuming pathways. An amount of 88% of NH_2 radicals tend to consume NO and produce N_2 through the chain-terminating reaction R18. Further, the kinetic mechanism of Nakamura shows another NO formation pathway (NH_3 $\rightarrow$ NH_2 $\rightarrow$ N_2H_2 $\rightarrow$ NO) at rich conditions which is not present in Wang's mechanism. The NO mole fraction increases by the reaction of N_2H_2 with high reactive O radicals through the kinetic reaction N_2H_2 + O $\rightleftharpoons$ NO + NH_2. Additionally, the kinetic schemes of both kinetic models show different concentrations of reactive radicals that tend to react with HNO, NH, and N to form NO.

Some of the kinetic reactions of Nakamura's model show higher levels of reactivity than those of Wang's model; see Figure 27. For example, the thermal NO reactions of the Zeldovich mechanisms R24 and R11 in NO formation [65]. Even though the activation energy of the former reaction (R24) is the same in both models, the system's temperature varies among the model's predictions. It positively affects the reactivity of the mentioned reactions. Similar observations can be drawn for the thermal NO reaction (R11) by including another affecting factor: activation energy. The latter reaction (R11) in Nakamura's model works as an independent temperature reaction (has zero activation energy). The case is not the same with the same kinetic reaction of Wang's model reaction with an activation energy equal to 49,500 cal/mol, making it a highly temperature-dependent reaction; see Table 3.

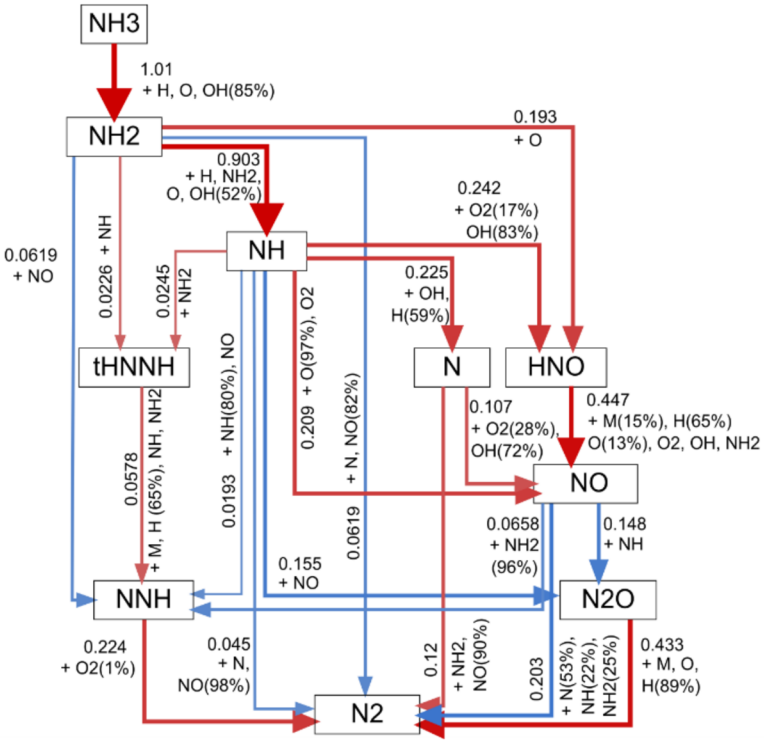

Z. Wang et al., [46] kinetic scheme

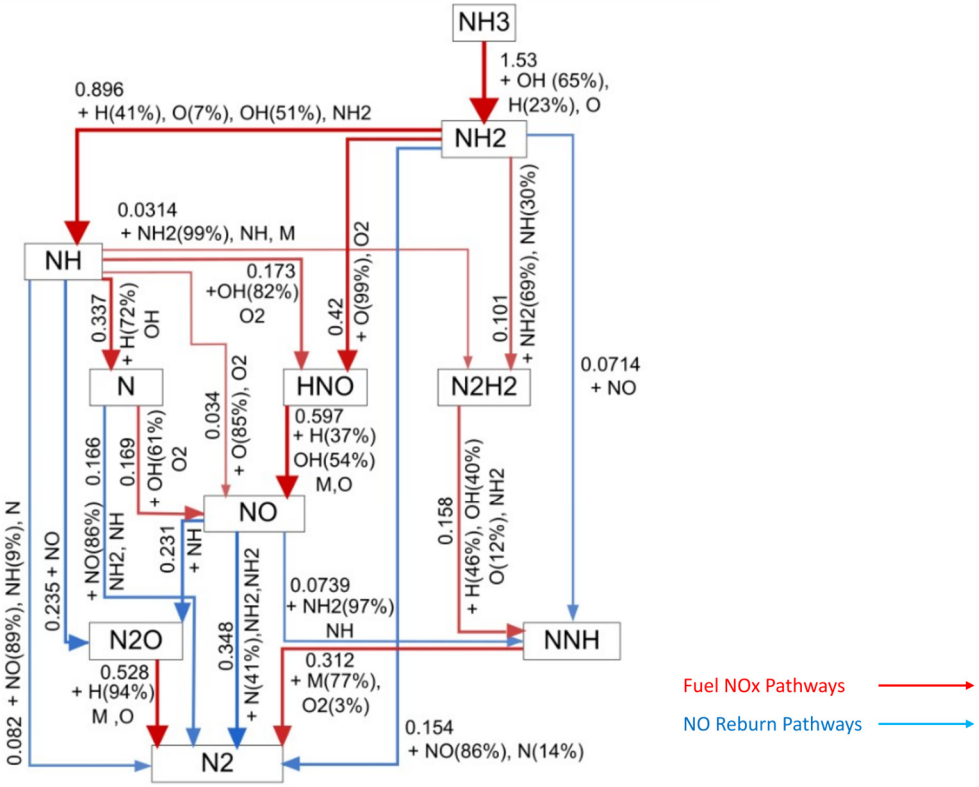

Nakamura et al., [69] kinetic scheme

Figure 26. Chemical reaction pathways of NO formation/consumption at flame zone (T = 1513 K) and at ϕ = 1.2 predicted by the Z. Wang et al., [46] and Nakamura et al., [69] kinetic models. Arrow lines refer to chemical transformations, percentages (%) show the contribution of a reactant to the transformation, numbers stand for the net reaction rate in kmol/m^{3}s, which is also visualized by line thickness.

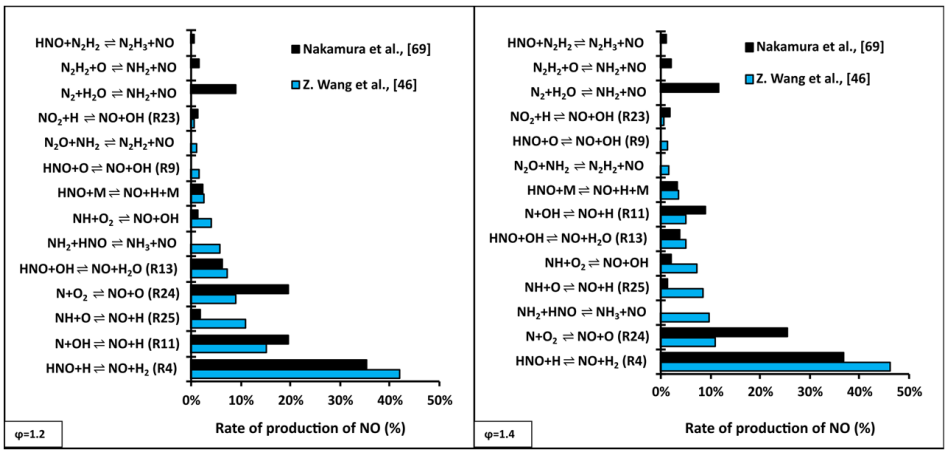

Figure 27. Rate of production of NO in (%) at rich conditions estimated by the Nakamura et al., [69] and Z. Wang et al., [46] kinetic models.

Figure 28 presents the values of the consumption rate of the most important kinetic reactions in NO consumption in terms of equivalence ratio. Most kinetic reactions in Wang's model demonstrate higher values than those in Nakamura's model. The kinetic reactions of the Zeldovich mechanism R26 and R22 depict higher values of NO consumption rate in Nakamura's model than in Wang's. The reason can be justified based on the Arrhenius parameters that governed these two reactions. As seen from Table 3, the Arrhenius parameters' values differ among the tested kinetic models, where the former reaction (R26) has positive activation energy, accelerating the system's reactivity as temperature increases. However, this is not the case for Wang's model, which shows negative activation energy values with opposite effects on temperature. The other Zeldovich reaction, 'R22', has different values listed among the selected mechanisms and shows independent temperature reaction in Nakamura's model and has a negative effect on reactivity when the system's temperature increases; see Table 3.

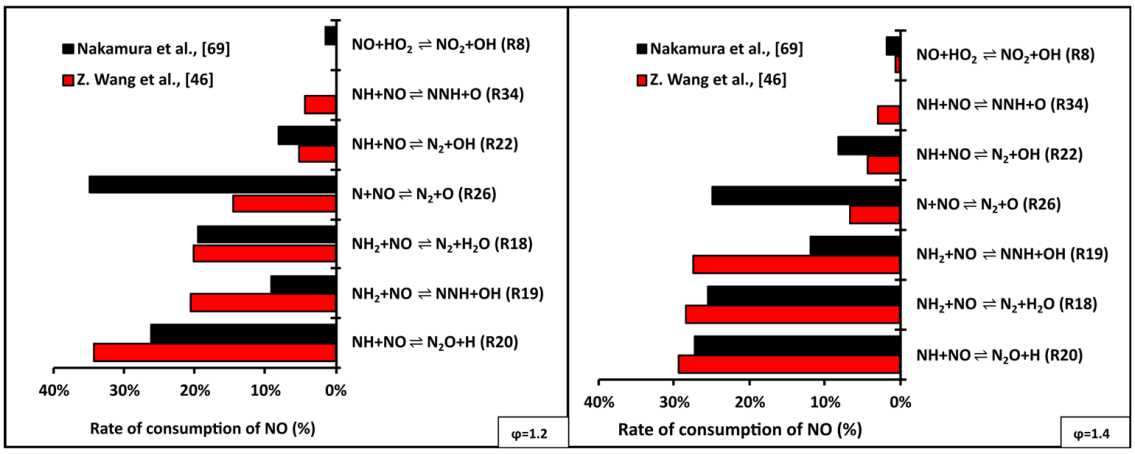

Figure 28. Rate of consumption of NO in (%) at rich conditions estimated by the Nakamura et al., [69] and Z. Wang et al., [46] kinetic models.

4. Conclusions

The present study investigated the formation/consumption of NO mole fraction for a 70/30 (vol%) NH_3/H_2 mixture at atmospheric conditions and a wide range of equivalence ratios (0.6–1.4). Different chemical kinetic reaction mechanisms (67) designed for ammonia combustion have been examined to assess their performance in NO prediction compared to experimental data from the literature. The main conclusion points are listed as follows:

1. Within the lean and stoichiometric range of equivalence ratios (0.6–1.0), Glarborg and Nakamura's mechanisms demonstrated strong predictive capabilities and closely approximated experimental measurements, exhibiting minimal discrepancies. Similarly, Wang's kinetic model yielded accurate estimations of the experimental data, although minor errors and deviations were observed at $\phi = 1.4$;
2. Under lean conditions in 70/30 (vol%) NH_3/H_2 mixture, the kinetic reactions HNO + OH $\rightleftharpoons$ NO + H_2O, HNO + H $\rightleftharpoons$ NO + H_2, N + O_2 $\rightleftharpoons$ NO + O, and N + OH $\rightleftharpoons$ NO + H were identified as the primary drivers of NO formation. Conversely, the reactions NH_2 + NO $\rightleftharpoons$ N_2 + H_2O, NH + NO $\rightleftharpoons$ N_2O + H, NH_2 + NO $\rightleftharpoons$ NNH + OH, NH + NO $\rightleftharpoons$ N_2 + OH, and N + NO $\rightleftharpoons$ N_2 + O were found to be the predominant NO-consuming reactions, leading to a reduction in the NO mole fraction;
3. Examination of lean flames demonstrated that the kinetic reactions HNO + H $\rightleftharpoons$ NO + H_2, HNO + O $\rightleftharpoons$ NO + OH, and NH + O $\rightleftharpoons$ NO + H are the primary contributors to NO formation. These reactions exhibit higher production rates in Glarborg's mechanism compared to Nakamura's kinetic model, thus contributing to the overestimation of NO by the former;
4. Under rich conditions, the kinetic reactions HNO + H $\rightleftharpoons$ NO + H_2, N + O_2 $\rightleftharpoons$ NO + O, NH_2 + HNO $\rightleftharpoons$ NH_3 + NO, and N + OH $\rightleftharpoons$ NO + H were identified as the primary drivers of NO production. Conversely, the reactions NH + NO $\rightleftharpoons$ N_2O + H, NH_2 + NO $\rightleftharpoons$ NNH + OH, NH_2 + NO $\rightleftharpoons$ N_2 + H_2O, and N + NO $\rightleftharpoons$ N_2 + O were found to be the main NO consumption reactions, leading to a decrease in NO mole fractions;
5. Upon analyzing the performance of the chosen kinetic mechanisms under rich conditions, it was found that the reactions N + O_2 $\rightleftharpoons$ NO + O, N + OH $\rightleftharpoons$ NO + OH, and N_2 + H_2O $\rightleftharpoons$ NH_2 + NO may account for the overestimation of NO production observed in Nakamura's kinetic model when compared to Wang's model. Specifically, the first two reactions are part of the NO thermal mechanism in the Zeldovich model and exhibit strong temperature dependence. Since Nakamura's model predicts a higher system temperature than Wang's, these reactions become more reactive, resulting in discrepancies in the predicted NO mole fractions;
6. The variation in NO mole fraction predictions between the studied kinetic models can be attributed to the distinct ways in which NO chemistry is represented among the chosen models.

Author Contributions: Conceptualization, A.A., H.S., A.H. and A.V.-M.; Methodology, A.A., S.M., A.H. and A.V.-M.; Software, A.A. and S.M.; Validation, A.A., S.M., M.H., A.H. and A.V.-M.; Formal analysis, A.A., J.J. and A.V.-M.; Investigation, A.A., S.M. and A.V.-M.; Resources, A.A., M.H., J.J. and A.H.; Data curation, A.A., M.H., H.S., A.H. and A.V.-M.; Writing—original draft, A.A.; Writing—review & editing, A.A., J.J., H.S., A.H. and A.V.-M.; Supervision, A.V.-M.; Project administration, A.V.-M.; Funding acquisition, A.V.-M. All authors have read and agreed to the published version of the manuscript.

Funding: The authors acknowledge the financial support of EPSRC through the projects SAFE-AGT Pilot (No. EP/T009314/1) and Green Ammonia Thermal Propulsion MariNH_3 (No. EP/W016656/1).

Data Availability Statement: Information on the data underpinning the results presented here, including how to access them, can be found in the Cardiff University data catalogue at http://doi.org/10.17035/d.2023.0253004071.

Acknowledgments: The authors gratefully acknowledge the support from EPSRC through the projects SAFE-AGT Pilot (No. EP/T009314/1) and Green Ammonia Thermal Propulsion MariNH_3 (No. EP/W016656/1), as well as Joanna Jójka, has received funding under a doctoral fellowship from the National Science Center, Poland, No. UMO-2019/32/T/ST8/00265. Furthermore, Ali Alnasif thanks Al-Furat Al-Awsat Technical University (ATU) for the financial support towards his Ph.D. studies in the UK. Information on the data underpinning the results presented here, including how to access them, can be found in the Cardiff University data catalogue at http://doi.org/10.17035/d.2023.0253004071.

Conflicts of Interest: The authors declare no conflict of interest.

References

1. Chen, J.; Fei, Y.; Wan, Z. The relationship between the development of global maritime fleets and GHG emission from shipping. *J. Environ. Manag.* **2019**, *242*, 31–39. [CrossRef] [PubMed]
2. Kojima, Y. Hydrogen storage materials for hydrogen and energy carriers. *Int. J. Hydrogen Energy* **2019**, *44*, 18179–18192. [CrossRef]
3. Valera-Medina, A.; Xiao, H.; Owen-Jones, M.; David, W.; Bowen, P. Ammonia for power. *Prog. Energy Combust. Sci.* **2018**, *69*, 63–102. [CrossRef]
4. Kobayashi, H.; Hayakawa, A.; Somarathne, K.K.A.; Okafor, E.C. Science and technology of ammonia combustion. *Proc. Combust. Inst.* **2019**, *37*, 109–133. [CrossRef]
5. Li, J.; Lai, S.; Chen, D.; Wu, R.; Kobayashi, N.; Deng, L.; Huang, H. A Review on Combustion Characteristics of Ammonia as a Carbon-Free Fuel. *Front. Energy Res.* **2021**, *9*, 760356. [CrossRef]
6. Chai, W.S.; Bao, Y.; Jin, P.; Tang, G.; Zhou, L. A review on ammonia, ammonia-hydrogen and ammonia-methane fuels. *Renew. Sustain. Energy Rev.* **2021**, *147*, 111254. [CrossRef]
7. Choi, S.; Lee, S.; Kwon, O. Extinction limits and structure of counterflow nonpremixed hydrogen-doped ammonia/air flames at elevated temperatures. *Energy* **2015**, *85*, 503–510. [CrossRef]
8. Somarathne, K.D.K.A.; Hatakeyama, S.; Hayakawa, A.; Kobayashi, H. Numerical study of a low emission gas turbine like combustor for turbulent ammonia/air premixed swirl flames with a secondary air injection at high pressure. *Int. J. Hydrog. Energy* **2017**, *42*, 27388–27399. [CrossRef]
9. Hayakawa, A.; Arakawa, Y.; Mimoto, R.; Somarathne, K.K.A.; Kudo, T.; Kobayashi, H. Experimental investigation of stabilization and emission characteristics of ammonia/air premixed flames in a swirl combustor. *Int. J. Hydrog. Energy* **2017**, *42*, 14010–14018. [CrossRef]
10. Mashruk, S.; Kovaleva, M.; Alnasif, A.; Chong, C.T.; Hayakawa, A.; Okafor, E.C.; Valera-Medina, A. Nitrogen oxide emissions analyses in ammonia/hydrogen/air premixed swirling flames. *Energy* **2022**, *260*, 125183. [CrossRef]
11. Alnasif, A.; Mashruk, S.; Kovaleva, M.; Wang, P.; Valera-Medina, A. Experimental and numerical analyses of nitrogen oxides formation in a high ammonia-low hydrogen blend using a tangential swirl burner. *Carbon Neutrality* **2022**, *1*, 1–20. [CrossRef]
12. Mashruk, S.; Kovaleva, M.; Tung Chong, C.; Hayakawa, A.; Okafor, E.C.; Valera-Medina, A. Nitrogen Oxides as a By-product of Ammonia/Hydrogen Combustion Regimes. *Chem. Eng. Trans.* **2021**, *89*, 613–618. [CrossRef]
13. Mashruk, S.; Kovaleva, M.; Zitouni, S.E.; Mounaim-Rouselle, C.; Valera-Medina, A. Ammonia/Hydrogen/Methane Characteristic Profiles for Atmospheric Combustion Applications. In Proceedings of the International Conference on Applied Energy 2021, Bangkok, Thailand, 29 November–2 December 2021.
14. Abián, M.; Benés, M.; de Goñi, A.; Muñoz, B.; Alzueta, M. Study of the oxidation of ammonia in a flow reactor. Experiments and kinetic modeling simulation. *Fuel* **2021**, *300*, 120979. [CrossRef]
15. Sullivan, N.; Jensen, A.; Glarborg, P.; Day, M.S.; Grcar, J.F.; Bell, J.B.; Pope, C.J.; Kee, R.J. Ammonia conversion and NOx formation in laminar coflowing nonpremixed methane-air flames. *Combust. Flame* **2002**, *131*, 285–298. [CrossRef]
16. Konnov, A.A. Implementation of the NCN pathway of prompt-NO formation in the detailed reaction mechanism. *Combust. Flame* **2009**, *156*, 2093–2105. [CrossRef]
17. Lindstedt, P.; Lockwood, F.C.; Selim, M.A. Detailed Kinetic Modelling of Chemistry and Temperature Effects on Ammonia Oxidation. *Combust. Sci. Technol.* **1994**, *99*, 253–276. [CrossRef]
18. Miller, J.A.; Bowman, C.T. Mechanism and modeling of nitrogen chemistry in combustion. *Prog. Energy Combust. Sci.* **1989**, *15*, 287–338. [CrossRef]
19. Miller, J.A.; Smooke, M.D.; Green, R.M.; Kee, R.J. Kinetic Modeling of the Oxidation of Ammonia in Flames. *Combust. Sci. Technol.* **1983**, *34*, 149–176. [CrossRef]
20. Konnov, A.A.; De Ruyck, J. Kinetic Modeling of the Thermal Decomposition of Ammonia. *Combust. Sci. Technol.* **2000**, *152*, 23–37. [CrossRef]
21. Lindstedt, R.P.; Selim, M.A. Reduced reaction mechanisms for ammonia oxidation in premixed laminar flames. *Combust. Sci. Technol.* **1994**, *99*, 277–298. [CrossRef]
22. Lindstedt, R.P.; Lockwood, F.C.; Selim, M.A. A Detailed Kinetic Study of Ammonia Oxidation. *Combust. Sci. Technol.* **1995**, *108*, 231–254. [CrossRef]
23. Stagni, A.; Cavallotti, C.; Arunthanayothin, S.; Song, Y.; Herbinet, O.; Battin-Leclerc, F.; Faravelli, T. An experimental, theoretical and kinetic-modeling study of the gas-phase oxidation of ammonia. *React. Chem. Eng.* **2020**, *5*, 696–711. [CrossRef]
24. Gotama, G.J.; Hayakawa, A.; Okafor, E.C.; Kanoshima, R.; Hayashi, M.; Kudo, T.; Kobayashi, H. Measurement of the laminar burning velocity and kinetics study of the importance of the hydrogen recovery mechanism of ammonia/hydrogen/air premixed flames. *Combust. Flame* **2021**, *236*, 111753. [CrossRef]
25. Shrestha, K.P.; Lhuillier, C.; Barbosa, A.A.; Brequigny, P.; Contino, F.; Mounaïm-Rousselle, C.; Seidel, L.; Mauss, F. An experimental and modeling study of ammonia with enriched oxygen content and ammonia/hydrogen laminar flame speed at elevated pressure and temperature. *Proc. Combust. Inst.* **2020**, *38*, 2163–2174. [CrossRef]
26. Tian, Z.; Li, Y.; Zhang, L.; Glarborg, P.; Qi, F. An experimental and kinetic modeling study of premixed $NH_3/CH_4/O_2$/Ar flames at low pressure. *Combust. Flame* **2009**, *156*, 1413–1426. [CrossRef]

27. Mei, B.; Zhang, J.; Shi, X.; Xi, Z.; Li, Y. Enhancement of ammonia combustion with partial fuel cracking strategy: Laminar flame propagation and kinetic modeling investigation of $NH_3/H_2/N_2$/air mixtures up to 10 atm. *Combust. Flame* **2021**, *231*, 111472. [CrossRef]
28. Li, R.; Konnov, A.A.; He, G.; Qin, F.; Zhang, D. Chemical mechanism development and reduction for combustion of $NH_3/H_2/CH_4$ mixtures. *Fuel* **2019**, *257*, 116059. [CrossRef]
29. Nozari, H.; Karabeyoğlu, A. Numerical study of combustion characteristics of ammonia as a renewable fuel and establishment of reduced reaction mechanisms. *Fuel* **2015**, *159*, 223–233. [CrossRef]
30. Zhang, X.; Moosakutty, S.P.; Rajan, R.P.; Younes, M.; Sarathy, S.M. Combustion chemistry of ammonia/hydrogen mixtures: Jet-stirred reactor measurements and comprehensive kinetic modeling. *Combust. Flame* **2021**, *234*, 111653. [CrossRef]
31. Szanthoffer, A.G.; Zsély, I.G.; Kawka, L.; Papp, M.; Turányi, T. Testing of NH_3/H_2 and NH_3/syngas combustion mechanisms using a large amount of experimental data. *Appl. Energy Combust. Sci.* **2023**, *14*, 100127. [CrossRef]
32. Hayakawa, A.; Hayashi, M.; Kovaleva, M.; Gotama, G.J.; Okafor, E.C.; Colson, S.; Mashruk, S.; Valera-Medina, A.; Kudo, T.; Kobayashi, H. Experimental and numerical study of product gas and N_2O emission characteristics of ammonia/hydrogen/air premixed laminar flames stabilized in a stagnation flow. *Proc. Combust. Inst.* **2022**. [CrossRef]
33. Hayakawa, A.; Hayashi, M.; Gotama, G.J.; Kovaleva, M.; Okafor, E.C.; Colson, S.; Kudo, T.; Mashruk, S.; Valera-Medina, A.; Kobayashi, H. N_2O Production Characteristics of Ammonia/Hydrogen/Air Premixed Laminar Flames Stabilized in Stagnation Flows at Lean Conditions. In Proceedings of the 13th Asia-Pacific Conference on Combustion (ASPACC), Abu Dhabi, United Arab Emirates, 4–9 December 2021.
34. Hayakawa, A.; Hirano, Y.; Okafor, E.C.; Yamashita, H.; Kudo, T.; Kobayashi, H. Experimental and numerical study of product gas characteristics of ammonia/air premixed laminar flames stabilized in a stagnation flow. *Proc. Combust. Inst.* **2021**, *38*, 2409–2417. [CrossRef]
35. Flores, B.E. A pragmatic view of accuracy measurement in forecasting. *Omega* **1986**, *14*, 93–98. [CrossRef]
36. Syntetos, A.A.; Boylan, J.E. *Intermittent Demand Forecasting: Context, Methods and Applications*; John Wiley & Sons: Hoboken, NJ, USA, 2021.
37. Bertolino, A.; Fürst, M.; Stagni, A.; Frassoldati, A.; Pelucchi, M.; Cavallotti, C.; Faravelli, T.; Parente, A. An evolutionary, data-driven approach for mechanism optimization: Theory and application to ammonia combustion. *Combust. Flame* **2021**, *229*, 111366. [CrossRef]
38. Dagaut, P.; Glarborg, P.; Alzueta, M.U. The oxidation of hydrogen cyanide and related chemistry. *Prog. Energy Combust. Sci.* **2008**, *34*, 1–46. [CrossRef]
39. Mei, B.; Ma, S.; Zhang, X.; Li, Y. Characterizing ammonia and nitric oxide interaction with outwardly propagating spherical flame method. *Proc. Combust. Inst.* **2020**, *38*, 2477–2485. [CrossRef]
40. Smith, G.P.; Golden, D.M.; Frenklach, M.; Moriarty, N.W.; Eiteneer, B.; Goldenberg, M.; Bowman, C.T.; Hanson, R.K.; Song, S.W.C.; Gardiner, V.V.L., Jr.; et al. GRI-Mech 3.0. 2000. Available online: http://combustion.berkeley.edu/gri-mech/ (accessed on 23 April 2023).
41. Han, X.; Lavadera, M.L.; Konnov, A.A. An experimental and kinetic modeling study on the laminar burning velocity of NH_3+N_2O+air flames. *Combust. Flame* **2021**, *228*, 13–28. [CrossRef]
42. Zabetta, E.C.; Hupa, M. A detailed kinetic mechanism including methanol and nitrogen pollutants relevant to the gas-phase combustion and pyrolysis of biomass-derived fuels. *Combust. Flame* **2008**, *152*, 14–27. [CrossRef]
43. Alzueta, M.U. Zaragoza-2016 Mechanism. (Zaragoza University, Aragón, Spain). Personal Communication, 2016.
44. Shmakov, A.; Korobeinichev, O.; Rybitskaya, I.; Chernov, A.; Knyazkov, D.; Bolshova, T.; Konnov, A. Formation and consumption of NO in H_2+O_2+N_2 flames doped with NO or NH_3 at atmospheric pressure. *Combust. Flame* **2010**, *157*, 556–565. [CrossRef]
45. Esarte, C.; Peg, M.; Ruiz, M.P.; Millera, A.; Bilbao, R.; Alzueta, M.U. Pyrolysis of Ethanol: Gas and Soot Products Formed. *Ind. Eng. Chem. Res.* **2011**, *50*, 4412–4419. [CrossRef]
46. Wang, Z.; Han, X.; He, Y.; Zhu, R.; Zhu, Y.; Zhou, Z.; Cen, K. Experimental and kinetic study on the laminar burning velocities of NH_3 mixing with CH3OH and C2H5OH in premixed flames. *Combust. Flame* **2021**, *229*, 111392. [CrossRef]
47. Abian, M.; Alzueta, M.U.; Glarborg, P. Formation of NO from N_2/O_2Mixtures in a Flow Reactor: Toward an Accurate Prediction of Thermal NO. *Int. J. Chem. Kinet.* **2015**, *47*, 518–532. [CrossRef]
48. Wang, T.; Zhang, X.; Zhang, J.; Hou, X. Automatic generation of a kinetic skeletal mechanism for methane-hydrogen blends with nitrogen chemistry. *Int. J. Hydrogen Energy* **2018**, *43*, 3330–3341. [CrossRef]
49. Arunthanayothin, S.; Stagni, A.; Song, Y.; Herbinet, O.; Faravelli, T.; Battin-Leclerc, F. Ammonia–methane interaction in jet-stirred and flow reactors: An experimental and kinetic modeling study. *Proc. Combust. Inst.* **2020**, *38*, 345–353. [CrossRef]
50. Faravelli, T. POLIMI-2017. Personal Communication, 2017.
51. The CRECK Modeling Group. C1-C3 mechanism (Version 1412, December 2014). Available online: http://creckmodeling.chem.polimi.it/ (accessed on 23 April 2023).
52. Han, X.; Wang, Z.; Costa, M.; Sun, Z.; He, Y.; Cen, K. Experimental and kinetic modeling study of laminar burning velocities of NH_3/air, NH_3/H_2/air, NH_3/CO/air and NH_3/CH_4/air premixed flames. *Combust. Flame* **2019**, *206*, 214–226. [CrossRef]
53. Marques, C.; Dos Santos, L.R.; Sbampato, M.E.; Barreta, L.G.; Dos Santos, A.M. Temperature measurements by oh lif and chemiluminescence kinetic modeling for ethanol flames. *Quím. Nova* **2009**, *32*, 2073–2077. [CrossRef]

54. de Persis, S.; Pillier, L.; Idir, M.; Molet, J.; Lamoureux, N.; Desgroux, P. NO formation in high pressure premixed flames: Experimental results and validation of a new revised reaction mechanism. *Fuel* **2019**, *260*, 116331. [CrossRef]
55. Aranda, V.; Christensen, J.M.; Alzueta, M.U.; Glarborg, P.; Gersen, S.; Gao, Y.; Marshall, P. Experimental and Kinetic Modeling Study of Methanol Ignition and Oxidation at High Pressure. *Int. J. Chem. Kinet.* **2013**, *45*, 283–294. [CrossRef]
56. Mei, B.; Zhang, X.; Ma, S.; Cui, M.; Guo, H.; Cao, Z.; Li, Y. Experimental and kinetic modeling investigation on the laminar flame propagation of ammonia under oxygen enrichment and elevated pressure conditions. *Combust. Flame* **2019**, *210*, 236–246. [CrossRef]
57. Jiang, Y.; Gruber, A.; Seshadri, K.; Williams, F. An updated short chemical-kinetic nitrogen mechanism for carbon-free combustion applications. *Int. J. Energy Res.* **2019**, *44*, 795–810. [CrossRef]
58. Sun, J.; Yang, Q.; Zhao, N.; Chen, M.; Zheng, H. Numerically study of CH_4/NH_3 combustion characteristics in an industrial gas turbine combustor based on a reduced mechanism. *Fuel* **2022**, *327*, 124897. [CrossRef]
59. Okafor, E.C.; Naito, Y.; Colson, S.; Ichikawa, A.; Kudo, T.; Hayakawa, A.; Kobayashi, H. Measurement and modelling of the laminar burning velocity of methane-ammonia-air flames at high pressures using a reduced reaction mechanism. *Combust. Flame* **2019**, *204*, 162–175. [CrossRef]
60. Song, Y.; Marrodán, L.; Vin, N.; Herbinet, O.; Assaf, E.; Fittschen, C.; Stagni, A.; Faravelli, T.; Alzueta, M.; Battin-Leclerc, F. The sensitizing effects of NO2 and NO on methane low temperature oxidation in a jet stirred reactor. *Proc. Combust. Inst.* **2018**, *37*, 667–675. [CrossRef]
61. Glarborg, P.; Miller, J.A.; Ruscic, B.; Klippenstein, S.J. Modeling nitrogen chemistry in combustion. *Prog. Energy Combust. Sci.* **2018**, *67*, 31–68. [CrossRef]
62. Mével, R.; Javoy, S.; Lafosse, F.; Chaumeix, N.; Dupré, G.; Paillard, C.-E. Hydrogen–nitrous oxide delay times: Shock tube experimental study and kinetic modelling. *Proc. Combust. Inst.* **2009**, *32*, 359–366. [CrossRef]
63. Shrestha, K.P.; Seidel, L.; Zeuch, T.; Mauss, F. Detailed Kinetic Mechanism for the Oxidation of Ammonia Including the Formation and Reduction of Nitrogen Oxides. *Energy Fuels* **2018**, *32*, 10202–10217. [CrossRef]
64. da Rocha, R.C.; Costa, M.; Bai, X.-S. Chemical kinetic modelling of ammonia/hydrogen/air ignition, premixed flame propagation and NO emission. *Fuel* **2019**, *246*, 24–33. [CrossRef]
65. Otomo, J.; Koshi, M.; Mitsumori, T.; Iwasaki, H.; Yamada, K. Chemical kinetic modeling of ammonia oxidation with improved reaction mechanism for ammonia/air and ammonia/hydrogen/air combustion. *Int. J. Hydrogen Energy* **2018**, *43*, 3004–3014. [CrossRef]
66. Mechanism, U. *Chemical-Kinetic Mechanisms for Combustion Applications, Mechanical and Aerospace Engineering (Combustion Research)*; University of California at San Diego: San Diego, CA, USA, 2018.
67. Klippenstein, S.J.; Pfeifle, M.; Jasper, A.W.; Glarborg, P. Theory and modeling of relevance to prompt-NO formation at high pressure. *Combust. Flame* **2018**, *195*, 3–17. [CrossRef]
68. Kovaleva, M.; Hayakawa, A.; Colson, S.; Okafor, E.C.; Kudo, T.; Valera-Medina, A.; Kobayashi, H. Numerical and experimental study of product gas characteristics in premixed ammonia/methane/air laminar flames stabilised in a stagnation flow. *Fuel Commun.* **2022**, *10*, 100054. [CrossRef]
69. Nakamura, H.; Hasegawa, S.; Tezuka, T. Kinetic modeling of ammonia/air weak flames in a micro flow reactor with a controlled temperature profile. *Combust. Flame* **2017**, *185*, 16–27. [CrossRef]
70. Houshfar, E.; Skreiberg, Ø.; Glarborg, P.; Løvås, T. Reduced chemical kinetic mechanisms for NOx emission prediction in biomass combustion. *Int. J. Chem. Kinet.* **2012**, *44*, 219–231. [CrossRef]
71. Zhang, Y.; Mathieu, O.; Petersen, E.L.; Bourque, G.; Curran, H.J. Assessing the predictions of a NO x kinetic mechanism on recent hydrogen and syngas experimental data. *Combust. Flame* **2017**, *182*, 122–141. [CrossRef]
72. Lamoureux, N.; El Merhubi, H.; Pillier, L.; de Persis, S.; Desgroux, P. Modeling of NO formation in low pressure premixed flames. *Combust. Flame* **2016**, *163*, 557–575. [CrossRef]
73. Xiao, H.; Valera-Medina, A.; Bowen, P.J. Modeling Combustion of Ammonia/Hydrogen Fuel Blends under Gas Turbine Conditions. *Energy Fuels* **2017**, *31*, 8631–8642. [CrossRef]
74. Capriolo, G.; Brackmann, C.; Lavadera, M.L.; Methling, T.; Konnov, A. An experimental and kinetic modeling study on nitric oxide formation in premixed C3 alcohols flames. *Proc. Combust. Inst.* **2020**, *38*, 805–812. [CrossRef]
75. Song, Y.; Hashemi, H.; Christensen, J.M.; Zou, C.; Marshall, P.; Glarborg, P. Ammonia oxidation at high pressure and intermediate temperatures. *Fuel* **2016**, *181*, 358–365. [CrossRef]
76. Xu, L.; Chang, Y.; Treacy, M.; Zhou, Y.; Jia, M.; Bai, X.-S. A skeletal chemical kinetic mechanism for ammonia/n-heptane combustion. *Fuel* **2023**, *331*, 125830. [CrossRef]
77. Thomas, D.E.; Shrestha, K.P.; Mauss, F.; Northrop, W.F. Extinction and NO formation of ammonia-hydrogen and air non-premixed counterflow flames. *Proc. Combust. Inst.* **2022**, *in press*. [CrossRef]
78. Mathieu, O.; Petersen, E.L. Experimental and modeling study on the high-temperature oxidation of Ammonia and related NOx chemistry. *Combust. Flame* **2015**, *162*, 554–570. [CrossRef]
79. Kovács, M.; Papp, M.; Zsély, I.G.; Turányi, T. Determination of rate parameters of key N/H/O elementary reactions based on H_2/O_2/NOx combustion experiments. *Fuel* **2019**, *264*, 116720. [CrossRef]
80. Duynslaegher, C.; Contino, F.; Vandooren, J.; Jeanmart, H. Modeling of ammonia combustion at low pressure. *Combust. Flame* **2012**, *159*, 2799–2805. [CrossRef]

81. Kovács, M.; Papp, M.; Zsély, I.G.; Turányi, T. Main sources of uncertainty in recent methanol/NOx combustion models. *Int. J. Chem. Kinet.* **2021**, *53*, 884–900. [CrossRef]
82. Klippenstein, S.J.; Harding, L.B.; Glarborg, P.; Miller, J.A. The role of NNH in NO formation and control. *Combust. Flame* **2011**, *158*, 774–789. [CrossRef]
83. Zhang, K.; Li, Y.; Yuan, T.; Cai, J.; Glarborg, P.; Qi, F. An experimental and kinetic modeling study of premixed nitromethane flames at low pressure. *Proc. Combust. Inst.* **2011**, *33*, 407–414. [CrossRef]
84. Saxena, P.; Williams, F.A. Numerical and experimental studies of ethanol flames. *Proc. Combust. Inst.* **2007**, *31*, 1149–1156. [CrossRef]
85. Lamoureux, N.; Desgroux, P.; El Bakali, A.; Pauwels, J. Experimental and numerical study of the role of NCN in prompt-NO formation in low-pressure CH_4–O_2–N_2 and C_2H_2–O_2–N_2 flames. *Combust. Flame* **2010**, *157*, 1929–1941. [CrossRef]
86. Valkó, É.; Papp, M.; Kovács, M.; Varga, T.; Zsély, I.G.; Nagy, T.; Turányi, T. Design of combustion experiments using differential entropy. *Combust. Theory Model.* **2021**, *26*, 67–90. [CrossRef]
87. Alzueta, M.U.; Bilbao, R.; Finestra, M. Methanol Oxidation and Its Interaction with Nitric Oxide. *Energy Fuels* **2001**, *15*, 724–729. [CrossRef]
88. Mendiara, T.; Glarborg, P. Ammonia chemistry in oxy-fuel combustion of methane. *Combust. Flame* **2009**, *156*, 1937–1949. [CrossRef]
89. Nakamura, H.; Shindo, M. Effects of radiation heat loss on laminar premixed ammonia/air flames. *Proc. Combust. Inst.* **2019**, *37*, 1741–1748. [CrossRef]
90. Glarborg, P. The $NH_3/NO_2/O_2$ system: Constraining key steps in ammonia ignition and N_2O formation. *Combust. Flame* **2022**, 112311, *in press*. [CrossRef]